THESIS

OPTICAL PERFORMANCE OF CYLINDRICAL ABSORBER COLLECTORS WITH AND WITHOUT REFLECTORS

Submitted by

Arun B. Menon

Department of Mechanical Engineering

In partial fulfillment of the requirements

for the Degree of Master of Science

Colorado State University

Fort Collins, Colorado

Fall 1994

COLORADO STATE UNIVERSITY

July 31, 1994

WE HEREBY RECOMMEND THAT THE THESIS PREPARED UNDER OUR SUPERVISION BY ARUN B. MENON ENTITLED "OPTICAL PERFORMANCE OF CYLINDRICAL ABSORBER COLLECTORS WITH AND WITHOUT REFLECTORS" BE ACCEPTED AS FULFILLING IN PART REQUIREMENTS FOR THE DEGREE OF MASTER OF SCIENCE.

Committee on Graduate Work

Patrick J. Burns

David W. Yoder

Adviser

C. B. Winn

Department Head

ABSTRACT OF THESIS

OPTICAL PERFORMANCE OF CYLINDRICAL ABSORBER COLLECTORS WITH AND WITHOUT REFLECTORS

The optical efficiency of a solar collector, which depends on the collector geometry and material properties (i.e., geometry and radiative properties of the cover, absorber and any reflector), contributes significantly towards its overall performance. This optical efficiency is directly proportional to the transmittance-absorptance or $\tau\alpha$ product for all possible angles of incidence. A 3-D Monte Carlo ray tracing technique is used to determine this $\tau\alpha$ product for evacuated tubular collectors (ETCs) with cylindrical absorbers in an effort to identify the most efficient optical design parameters. These collectors are asymmetric with respect to the incident solar radiation and their optical efficiencies are therefore difficult to estimate using any other method.

The collector geometry is modeled using constructive solid geometry (CSG). CSG allows the generation of complex collector shapes by combining simple primitive objects. The ray tracing algorithm tracks individual photons through the collector geometry to provide a means of obtaining the absorbed fraction for a particular angle of radiation incident on the collector plane. Incidence angle modifiers (IAMs), the ratio of the $\tau\alpha$ product at a particular set of longitudinal and transverse radiation incidence angles to the $\tau\alpha$ product at normal incidence are thereby obtained.

IAMs are calculated for variations in five different design parameters to determine the most advantageous geometries. It is found that diffusely reflecting back planes significantly enhance optical performance of tubular collectors. Verification of the ray

trace calculations is made by comparing with experimental results from the indoor solar simulator at CSU. TRNSYS predicted values of $\tau\alpha$ are within 1% of the ray trace results for normal incidence tests and within 7% for off-normal tests. Inaccuracies resulting from the use of a multiplicative technique wherein off-axis IAMs are obtained by a multiplicative combination of the biaxial IAMs are also addressed. The multiplicative approach is found to be very inaccurate for angles of incidence greater than 40°.

To further assess the relative advantages of tubular collectors over flat plate collectors and whether a reflective back plane is really necessary, the two types of collectors are modeled in a simple fashion and the amount of radiation that is available for collection by each is determined. Calculations show that reflectors would probably not be required for collector slopes in excess of 50°. However, for slope angles less than 50°, a reflector placed behind the tubes is beneficial.

Arun B. Menon
Mechanical Engineering Department
Colorado State University
Fort Collins, CO 80523
Fall 1994

ACKNOWLEDGEMENTS

Work, such as is needed to complete a thesis, is seldom accomplished by any singular effort on the part of the author. There are usually many people that make such an endeavor possible, and I thankfully admit that this thesis is not an exception. I am grateful first to my adviser Dr. William Duff, whose many suggestions and corrections were most helpful. To all my colleagues at the Solar Lab and the ME department, my thanks for all their help; Jeff Miller deserves special recognition, for helping with all my software and hardware problems, as well as lifting my spirits whenever necessary; Pete, Mike, Tina, Kannan, Charu, Ranjani and Vinod for always being there for me and for all the great times. Thanks also to Dr. Dave Zachmann for serving on my graduate committee and for making the time to meet with me at short notice.

Special thanks are due to Steve Dempsey, who developed all the distributed system software. With his help I was able to use the computing resources at the College of Engineering in an efficient and productive manner.

I am most indebted to Dr. Pat Burns, who selflessly devoted an incredible amount of his time towards helping me write, organize and make this thesis imminently more readable than it otherwise might have been.

Finally, I wish to thank my parents Usha and Bala, and my brothers Arjun and Vikram, who were all so close to me, across all those miles!

TABLE OF CONTENTS

LIST OF FIGURES

LIST OF TABLES

NOMENCLATURE

A	=	current absorbed fraction
CSG	=	constructive solid geometry
ETC	=	evacuated tubular collector
FPC	=	flat plate collector
F	=	fraction diffuse multiplier
HT	=	radiation on tilted surface (MJ/m^2)
IAM	=	incidence angle modifier
N	=	number of photons cast in simulation
n	=	index of refraction, number of tubes
P	=	probability of reflection
p	=	pitch (cm)
R	=	rotation angles (°)
S	=	scaling values (cm)
T	=	translation coordinates
r	=	component of polarized radiation
W	=	width of aperture plane (cm)
z	=	normal distribution coefficient

Greek Letters

α	=	absorptivity
β	=	angle of incidence in longitudinal direction, collector slope (°)
γ	=	angle of incidence in transverse direction (°)

δ	=	confidence interval width
ϕ	=	surface azimuth angle (°)
κ	=	extinction coefficient
θ	=	angle of incidence (°)
$\tau\alpha$	=	transmittance-absorptance product
ρ	=	reflectivity

Subscripts

a	=	aperture
bp	=	back plane
D	=	diffuse
i	=	cell location in matrix
n	=	normal
w	=	width
1,2	=	refers to different media
$\perp$	=	perpendicular
$\parallel$	=	parallel
reflection	=	reflection
x,y,z	=	point coordinates

CHAPTER ONE

INTRODUCTION

1.1 Overview

A solar (thermal) collector is a device which intercepts radiant energy from the sun, converts it to thermal energy, and transfers the thermal energy to a circulating fluid. The performance of a solar collector depends on many quantities, including

- Climatic conditions: ambient temperature, wind, insolation
- Number of covers and their radiative properties (reflectance, absorptance)
- Incident solar angle
- Radiative properties of the absorber (absorptance and emittance), and its geometry (e.g., flat or cylindrical)
- Spacing of covers and absorber
- Fluid type, flow rate and fluid passage area
- Insulation of collector enclosure (e.g., airspace, evacuated)

The optical performance of a solar collector, which depends on the collector geometry and material properties (i.e., geometry and radiative properties of the cover, absorber and any reflector), contributes significantly to its overall performance. This optical performance is proportional to the $\tau\alpha$ or transmittance-absorptance product for all possible angles of incidence. The $\tau\alpha$ product is the fraction of the incident radiation transmitted through the cover assembly and eventually absorbed by the collector plate/tube. The $\tau\alpha$ value includes all interactions among the absorber, covers and reflectors (if present), and all effects of absorption by the covers. For flat-plate collectors (FPCs), determination of this $\tau\alpha$ product may be made in a relatively simple fashion using analytical relations.

However, for more complex geometries, and especially for asymmetric collectors, the $\tau\alpha$ product is much more difficult to estimate. Evacuated tubular collectors (ETCs) with cylindrical absorbers are one type of asymmetric solar collector, the characteristics of which are discussed in the following section. This thesis is devoted to the study of the optical performance of this type of collector in an effort to identify the most efficient design.

Knappmiller [1990] used a three dimensional technique to compute the fraction of solar radiation absorbed at any incident angle. His method employs a Monte Carlo approach, which involves the tracing of many individual rays through the collector geometry, to eventually determine the absorbed fraction. This procedure will be discussed in detail in later sections. The work in this thesis uses essentially the same technique, with some modifications to the original computer code and implementation scheme.

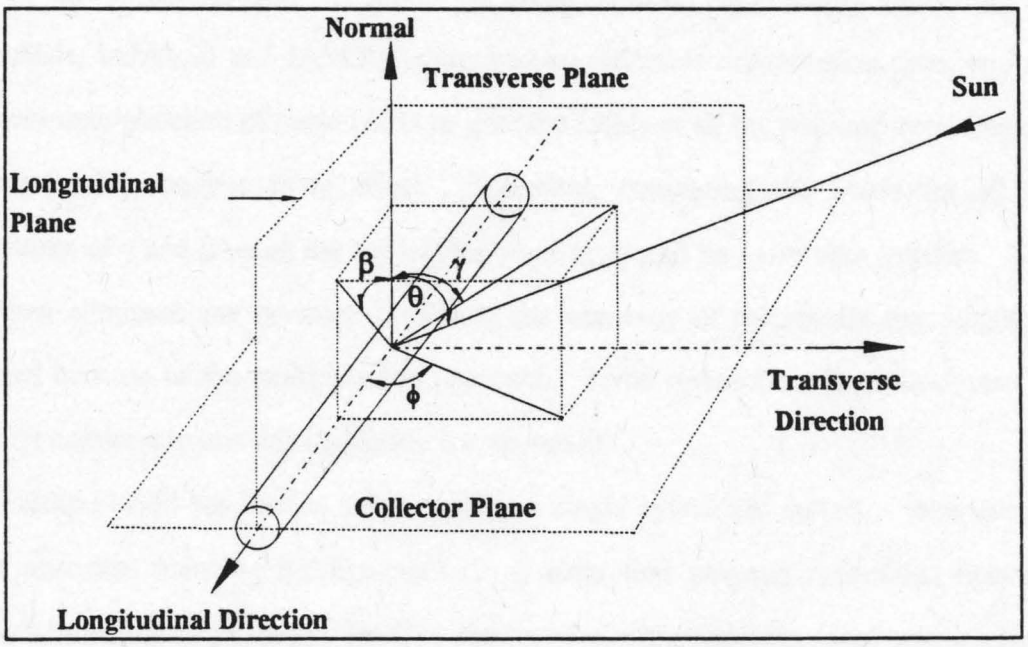

Figure 1.1 Angles γ and β with Respect to Collector Geometry

1.2 Literature Review

There has been a considerable amount of work devoted to the assessment of the optical performance characteristics of cylindrical absorber tubular collectors with and without back reflectors. There is currently no analytical approach developed which is adequate for the calculation of such characteristics. Further, it is difficult to obtain accurate experimental data of the fraction of radiation collected for various geometries. Hence, a simulation approach has been employed by many researchers.

McIntyre [1982] proposed a multiplicative approach, wherein the incidence angle modifier (IAM) at some combination of γ and β (defined in Fig. 1.1) may be approximated by multiplying the biaxial incidence angle modifiers, IAM(γ,0) and IAM(0,β).

$$IAM(\gamma,\beta) = IAM(\gamma,0)\ IAM(0,\beta) \qquad (1.1)$$

Use of the multiplicative approach can result in errors, as has been shown by Knappmiller [1990]. This has been confirmed in this thesis work. It does however result in some savings in computational time. It should be noted however, that simply computing the biaxial IAMs, IAM(γ,0) and IAM(0,β), requires considerable computation time, and the subsequent multiplication of these IAMs to give the IAMs at all the required combinations of γ and β also requires some effort. Therefore, computing the IAMs for all the combinations of γ and β using the ray tracing routine, would be more than justified. This would then eliminate any question regarding the accuracy of the results that might be introduced because of the multiplicative approach. Some researchers (e.g. Kaufmann, et al. [1993]) continue to use this multiplicative approach.

Felske [1979] has limited his analysis to a single cylindrical collector tube using a thin flat absorber spanning its diameter. It is clear that multiple reflections between successive tubes are neglected. This fact can be of significance when analyzing multiple tubes placed next to one another, or with the placement of a reflecting back surface.

Window and Zybert [1981], using a Monte Carlo ray tracing technique, have calculated the fractions of solar radiation collected by arrays of cylindrical absorbers with

diffuse reflectors of various shapes. The actual process by which the rays are traced through the collector geometry is quite similar to the method used in the program discussed in this thesis. Their program accounts for the fact that reflectance, transmittance and absorptance of surfaces depend on the angle of incidence and polarization of incoming radiation, and that radiation reflected from a module can be absorbed by that or another module. However, the angular distributions of input radiation used by them are limited to four different types, viz., hemispherical incidence (totally diffuse), arc incidence across tubes, arc incidence along tubes and normal incidence. The collection efficiencies for each of these radiation sources are presented, but total optical efficiencies (taking into consideration all possible types of incident radiation) are not addressed. Hence, evaluation of the optical performance at all possible angles of incoming radiation may not be possible.

Theunissen and Beckman [1985] have developed correlations of ray tracing results to compute transmittance for beam, sky and ground for a wide range of ETC designs. They compute longitudinal and transverse incidence angle modifiers as specified in testing standards, and in order to obtain the transmittance at any angle, they use McIntyre's multiplicative approach. Most significant is the fact that they assume the collector array to be infinite in both longitudinal and transverse directions so as to eliminate edge effects. Further, they also assume that the wall thickness of the glass tube is negligible compared to its diameter, and hence, assume that the rays are not displaced when passing through the glass.

In an effort to eliminate the inadequacies present in the methods discussed above, the approach used in this thesis work is designed to be applicable to a wide variety of asymmetric collector configurations. The important similarities/differences between the above methods and the ones used in this thesis work are discussed in the following section.

1.3 Scope of this Work

In contrast to the approaches mentioned above, the program used in this thesis uses direct beam input from a grid covering one quadrant of the hemisphere above the collector, thereby enabling the calculation of optical performance for all possible angles of incidence. The contribution of diffuse radiation (sky and ground) is then calculated by weighting IAMs at various angles of incidence.

The assumption of an infinite array is a major shortcoming and, in fact, the method used in this thesis analyzes collector geometries in a very realistic fashion. It is therefore possible to determine the edge effects which have otherwise been impossible to analyze using an analytical approach.

The thickness of the glass tubes is treated as finite, and absorption within the glass as well as refraction at the glass-air interfaces is modeled.

The results obtained by McIntyre's multiplicative method are compared to those obtained by computing the total hemispherical IAMs, i.e., the IAMs corresponding to all the combinations of γ and β used in the input file. Thus the errors obtained using the multiplicative method are presented.

Absorptivity and reflectivity of the materials are assumed to be constant with respect to varying angle of incidence. For some geometries this assumption may introduce significant error (Toor and Viskanta, [1967]). However, for the geometries analyzed in this thesis, this assumption appears to yield sufficiently accurate results. In the event that other geometries are to be modeled, where such an assumption may cause the analysis to fail badly, the program could be modified without significant effort to account for the directional properties.

CHAPTER TWO

PROBLEM DESCRIPTION

2.1 Theoretical Formulation

As discussed in the previous section, the aim of this work is the calculation of the optical performance of various solar collector geometries, which in turn is dependent on the $\tau\alpha$ product. This $\tau\alpha$ product as defined with respect to the ray-tracing simulation is,

$$\tau\alpha(\gamma,\beta) = \frac{\text{no. of rays absorbed by collector}}{\text{no. of rays hitting collector aperture plane}} \qquad (2.1)$$

where γ and β are the angles of incidence in the transverse and longitudinal planes as shown in Fig. 1.1, where these angles are illustrated with respect to the collector geometry.

Having defined the $\tau\alpha$ product (absorbed fraction), we can now define the biaxial Incidence Angle Modifier or, simply, the IAM as:

$$\text{IAM}(\gamma,\beta) = \frac{\tau\alpha(\gamma,\beta)}{\tau\alpha(0,0)} \qquad (2.2)$$

At normal incidence the transmittance-absorptance product is $\tau\alpha(0,0)$ or alternately $(\tau\alpha)_n$. The IAMs are thus a measure of the augmentation or attenuation in absorbed radiation (compared to that at normal incidence) for off-angle incidence. IAMs are directly used as weighting factors for beam radiation and may be used to compute diffuse fraction multipliers as well. This computation will be presented in a later section. These factors are needed in any global performance calculation, such as done in the TRNSYS (Klein [1992]) simulation program.

2.2 Geometry Studied

Cylindrical absorber tubular collectors (which are one kind of ETC) are the geometries studied in this thesis work. The base geometry analyzed is the NEG Sun Family Collector module, which consists of four cylindrical absorbers, each within an evacuated glass tube. This geometry is shown in Fig. 2.1. The important dimensions and material properties of the main collector parts are presented in Table 2.1.

Cover:
- Material: Glass (Tubular Construction)
- Length: 201.6 cm
- Outside Diameter: 12.6 cm
- Thickness: 0.2 cm
- Index of Refraction (n): 1.526
- Extinction Coefficient (κ): 0.004

Absorber:
- Material: Copper with Black Chrome Selective Coating (Cylindrical Construction)
- Length: 201.0 cm
- Diameter: 11.0 cm
- Absorptivity (α): 0.91

Reflector:
- Material: White Paint on Wood
- Reflectivity (ρ): 0.8 (100 % Diffuse)

Table 2.1 Relevant Dimensions and Material Properties of Main Collector Parts

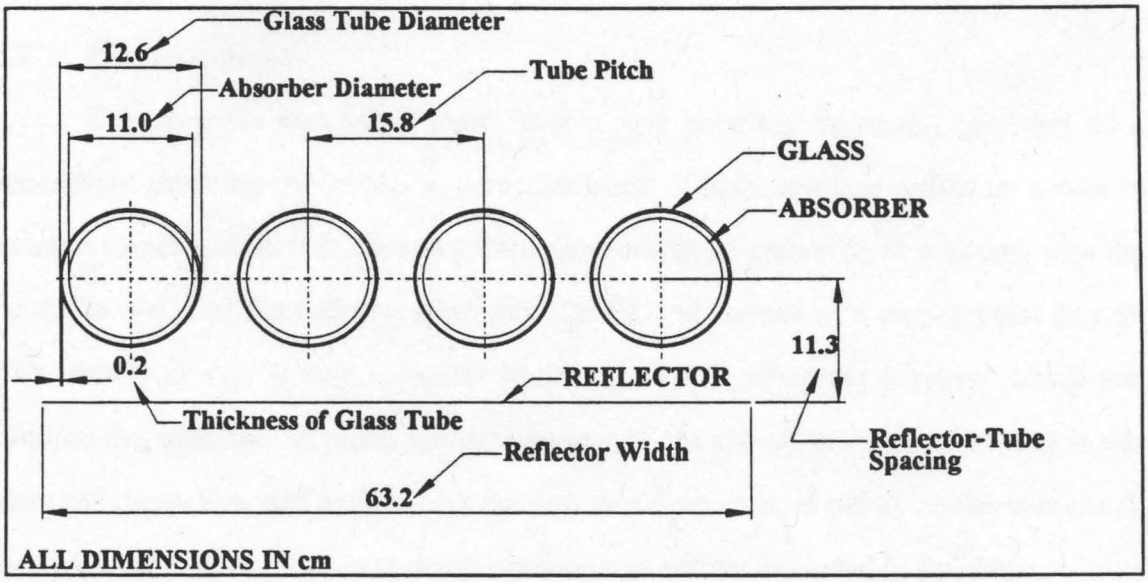

Figure 2.1 NEG Sun Family Collector Base Geometry

In order to determine advantageous design parameters for a given collector configuration, IAMs are calculated for variations in the following design parameters:

- back plane reflectance
- back plane width
- number of tubes/modules
- inter-tube spacing
- back plane to tube spacing

All of the above factors significantly affect the performance of this type of collector. Reflective back planes may not necessarily result in enhanced optical efficiencies. Placing a reflective surface behind a tubular collector restricts its collection of radiation coming from the back of the collector (i.e., $\theta > 90°$). A method has been developed to determine the amount of collection possible from the back. Comparing this information with the IAM results it is then possible to determine if using a reflective surface behind the tubes enhances performance of the collector. The question of the optimal placement of the reflector is answered by analyzing the ray trace results where the back plane to tube spacing is varied.

2.3 Program Input

The program uses beam input from a grid covering the entire quadrant of a hemisphere above the collector. A particular angle of incidence is specified by means of an input vector, which is defined in a Cartesian coordinate system by two points, with the tip at the center of the collector geometry (0,0,0), and the tail at a second point (x,y,z). This vector, or ray, is then extended backward until it intersects a sphere which just contains the collector. A plane, which is tangent to the sphere, is then constructed at this point of intersection, and parallel rays are then cast from random points on this plane back towards the collector. The ray tracing methodology will be discussed in detail later.

The input to the program is therefore a data file which consists of the X, Y and Z axis coordinates of the tail points for the input vectors. These coordinates may be generated in two ways. The first method, developed by Knappmiller [1990], consists of specifying an angular increment for the generation of various grid points. The angle of incidence from the vertical, θ, is first incremented by the angular increment specified, and then the azimuth angle ϕ is incremented by the same amount. This is done for $0° \leq \theta < 90°$, and for $0° \leq \phi < 90°$. The X, Y and Z coordinates of the points corresponding to each combination of θ and ϕ are then obtained by using the following relations:

$$z = \left| \frac{1}{\tan^2(\theta) + 1} \right| \tag{2.3}$$

$$y = \left| \frac{1}{\tan^2(\phi) + 1} \right| \tag{2.4}$$

$$x = |1 - z - y| \tag{2.5}$$

In this fashion it is possible to create a hemispherical grid, in which the number of points depends on the angular increment desired. The distribution of input vector origins for a 5° increment using this method is shown in Fig. 2.2.

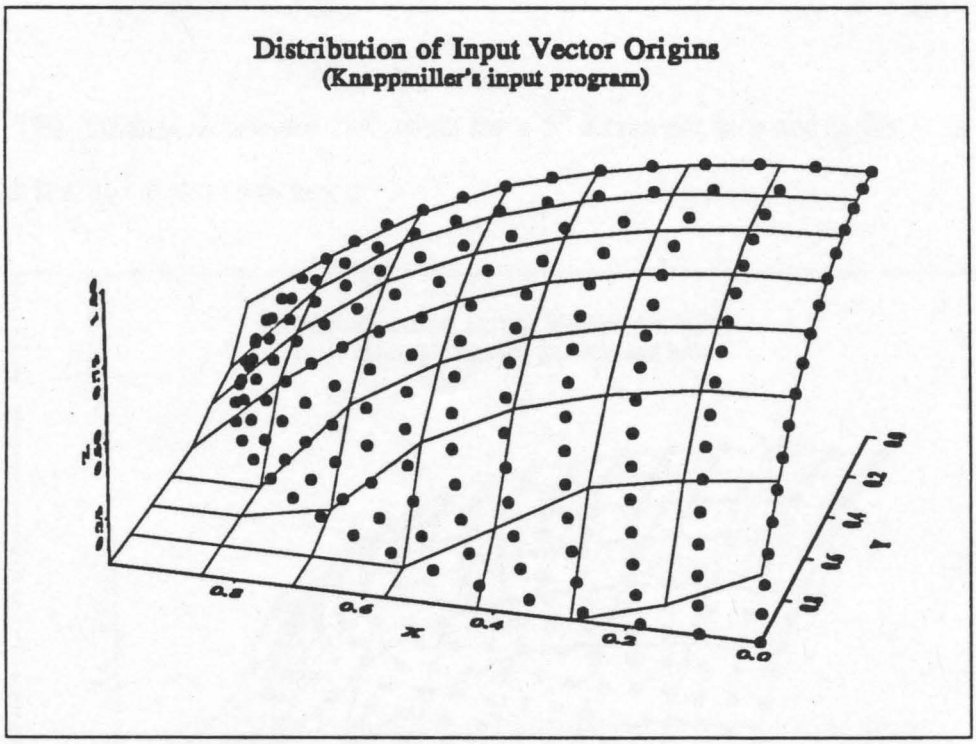

Figure 2.2 Knappmiller's Distribution of Input Vector Origins

Although the method described above provides a grid uniformly spaced in θ and ϕ, the angles γ and β associated with each point do not form a regular distribution that can allow the IAMs corresponding to each input direction to be easily incorporated in the form of a matrix. For this purpose, another method was developed to provide a list of input vector coordinates, corresponding to a uniform angular increment of γ and β. Thus for a uniformly increasing set of angles γ and β, the necessary X, Y and Z coordinates of the unit direction vector may be obtained using the following relations:

$$x = \sqrt{\frac{-(\sin^2(\gamma)\sin^2(\beta)) + \sin^2(\gamma)}{1-(\sin^2(\gamma)\sin^2(\beta))}} \tag{2.6}$$

$$y = \sqrt{\frac{-(\sin^2(\gamma)\sin^2(\beta)) + \sin^2(\beta)}{1-(\sin^2(\gamma)\sin^2(\beta))}} \tag{2.7}$$

$$z = \sqrt{1-(x^2+y^2)} \tag{2.8}$$

The resultant distribution of points for a 5° increment in γ and b, for $0° \leq \gamma \leq 85°$ and $0° \leq \beta \leq 85°$ is shown in Fig. 2.3.

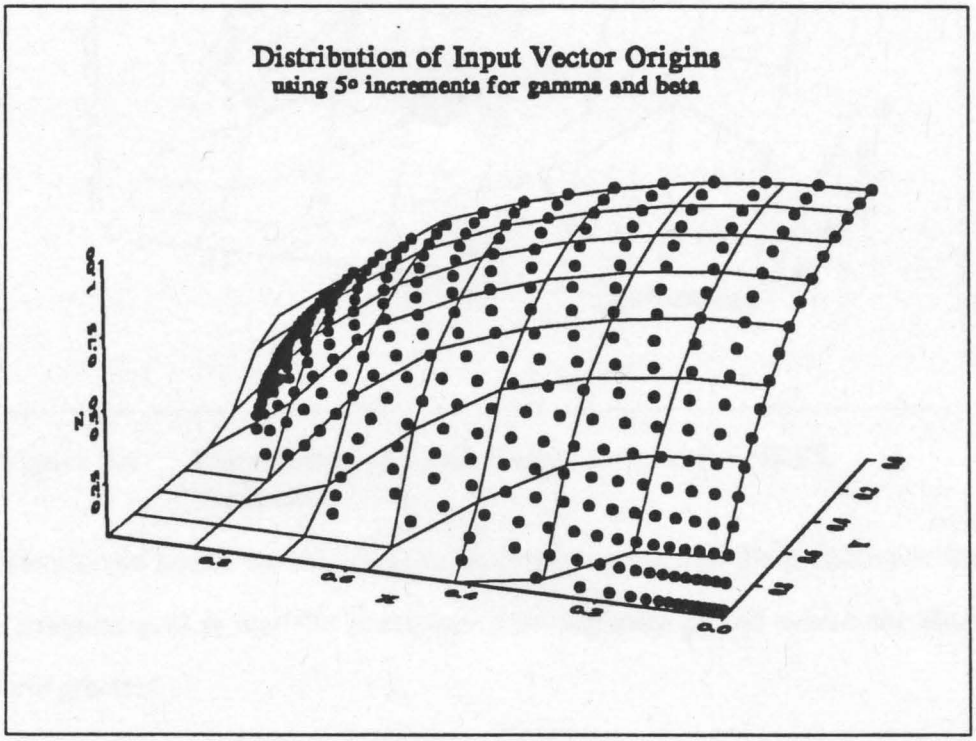

Figure 2.3 Distribution of Input Vector Origins Developed for this Thesis

This method does not yield as good a spatial distribution of points as the previous method, but it lends itself very easily for the incorporation of IAMs in the form of a regular matrix in terms of γ and β.

A subset of the data set plotted above is used to supply researchers at the National Renewable Energy Laboratory (NREL) with a matrix of IAMs for various collector geometries. The IAM matrix is used as input to TRNSYS, for purposes of simulation. Fig. 2.4 shows the distribution of points for the NREL requested data set.

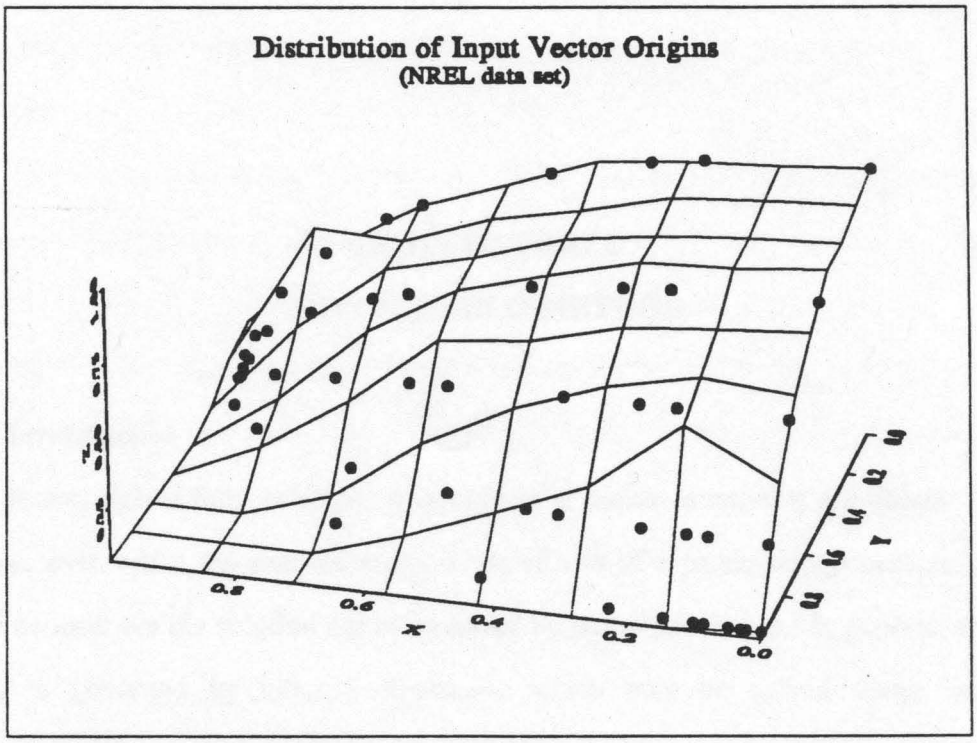

Figure 2.4 Distribution of Input Vector Origins for NREL Data Set

The distribution of points for this data set is very irregular and the justification for using such an irregular grid is that the points were strategically placed where the changes in IAMs were greatest.

2.4 Surface Description

The program is capable of modeling two types of surfaces, opaque and transparent. Opaque surfaces may be either absorbers, reflectors (purely diffuse or specular, or partly diffuse and partly specular), or surfaces which are neither absorbers or reflectors, but are simply part of the collector geometry.

Transmissive surfaces, such as glass, are treated very realistically, and refraction and absorption within the glass are modeled.

The required input parameters for surface and the actual outcome of the path of a ray when it encounters a surface will be described in later sections.

CHAPTER THREE

MONTE CARLO METHOD

3.1 Introduction

Exact, closed form solutions to problems in radiative transfer are usually difficult to obtain, even when the analysis neglects the effects of a participating medium. Under most circumstances the solution has to be found by numerical means. In general, radiative transfer is governed by integral equations, which may be solved using numerical quadrature for the evaluation of integrals. With these techniques the solutions to relatively simple problems are readily found. However, if the geometry is complicated, or the transport of radiation involves multiple interactions, then a solution by conventional numerical techniques may be difficult or impossible.

Many mathematical problems may be solved by statistical sampling techniques to a desired degree of accuracy. Solving mathematical problems statistically may involve the use of random numbers, which are generated by some random process. An example of such a process is placing a ball into a spinning roulette wheel. Hence, these sampling methods are often called *Monte Carlo* methods (named after the principality of Monte Carlo in the south of France, famous for its casinos). There is no general agreement as to the various numerical sampling schemes that the name Monte Carlo applies.

Problems in radiation are particularly well suited to solution by a Monte Carlo approach, since energy travels in the form of discrete particles, photons, over distances that are usually relatively long, along, usually, straight paths before interaction with matter. Solving a radiation problem by Monte Carlo methods implies tracing a statistically

meaningful random sample of photons from their points of emission to their points of absorption.

The major motivating factor for the use of the Monte Carlo method is that even the most complicated problems may be solved with relative ease. This is schematically indicated in Fig. 3.1, taken from Modest [1993]. For problems beyond a certain complexity of formulation, the Monte Carlo solution is preferable to those using conventional methods. Unfortunately, there is usually no way to determine where this crossover point in complexity lies, and researchers have to rely on experience.

Monte Carlo methods also generally produce an estimate of the calculation error.

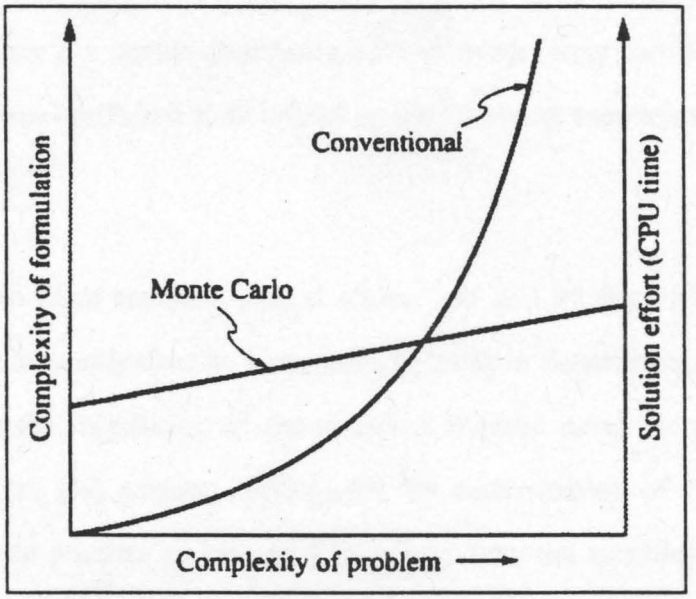

Figure 3.1 Comparison of Monte Carlo and Conventional Solution Techniques (From Modest)

3.2 Accuracy and Convergence

The main objective of the program used here, as mentioned earlier, is to determine the $\tau\alpha$ product of a specified collector geometry at various angles of incidence. This

involves tracing the path of numerous photons as they pass through the collector geometry to determine whether they eventually get absorbed by the absorber tube. A photon may sometimes interact with many intermediate surfaces before it even hits an absorber tube, and an accurate answer to such a problem can be determined only if a sufficiently large number of photons are cast in the simulation and if the simulation is allowed to carry on for a reasonably long time. The time a simulation requires is dependent on the maximum number of interactions that a photon is allowed to have before its ray trace is terminated. If this number is set to too low a value, then the absorbed fraction obtained will also be significantly lower than the true value.

For a Monte Carlo simulation of this type, Maltby [1990] has shown that for a current absorbed fraction A ($\tau\alpha$ in this thesis), and number of photons cast in the simulation N, there is a certain confidence interval width (error band) δ with a cumulative normal distribution coefficient z, all related by the following expression:

$$\delta = z\sqrt{\frac{1-A}{NA}} \tag{3.1}$$

where z is taken from standard normal tables, and is 1.96 for 95% confidence. This relation was subsequently used by Knappmiller [1990] in determining the confidence level associated with the calculation of the absorbed fraction using his program. The user specifies a percent (%) accuracy desired for the determination of $\tau\alpha$, and the program continues to trace photons as long as δ is greater than the specified accuracy. A more detailed treatment of Equation (3.1) may be obtained from Maltby [1990].

The statistical sampling in this simulation is done with the help of a numerical algorithm called a pseudorandom number generator. This type of generator, after a choice of a starting point or *seed* has been made, generates a new pseudorandom number from the previous one. Each initial seed creates a different sequence of random numbers, so different answers are obtained. However, if "enough" photons are cast in the simulation to achieve convergence, the answers, whatever the initial seed, will be identical to within a

statistical convergence error. Knappmiller (for one particular collector), has displayed the error and confidence related by Equation (3.1) associated with using different initial seeds by plotting the current fraction absorbed A, against the number of photons cast in the simulation N for several initial seeds. He has also shown the continuing convergence of the current fraction absorbed to be within the limits of Equation (3.1). Similar tests of convergence were performed for one of the geometries analysed in this thesis, the results of which are shown in Figs. 3.2 and 3.3. Further, he showed that single precision accuracy of the computer was sufficient for such a computation.

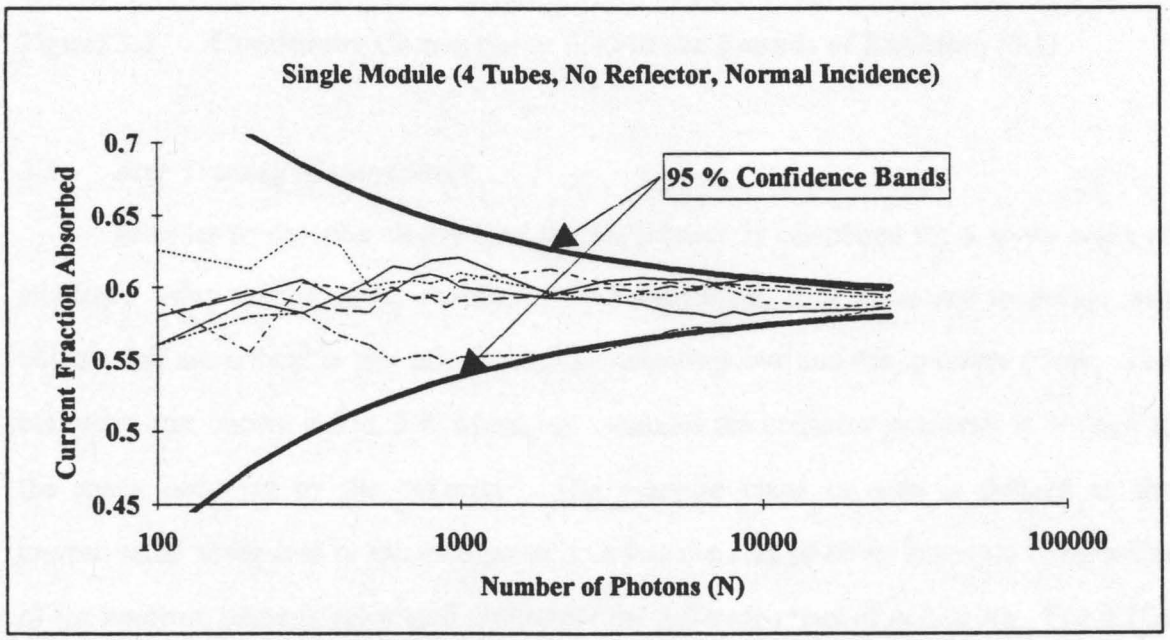

Figure 3.2 Effect of Initial Seeds on Current Fraction Convergence

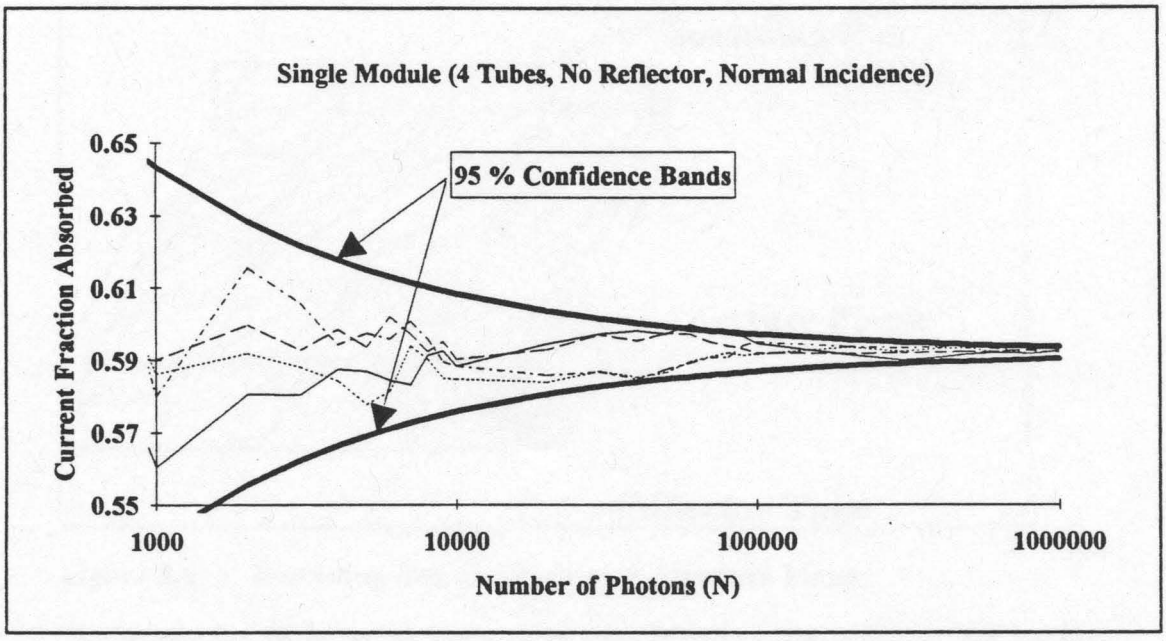

Figure 3.3 Continuing Convergence Within the Bounds of Equation (3.1)

3.3 Ray Tracing Methodology

In order to describe clearly how the $\tau\alpha$ product is calculated for a given angle of incidence using the technique developed by Knappmiller, it is necessary to define two objects that are critical in this calculation, the *bounding box* and the *aperture plane*. The bounding box, shown in Fig. 3.4, which just contains the collector geometry is defined as the space occupied by the collector. The aperture plane or area is defined as the unobstructed cover area or the total cover area less the area of cover supports. The width of the aperture plane is calculated differently for different types of collectors. For ETCs the width of the aperture plane is calculated as:

$$W_a = np \tag{3.2}$$

where n is the number of tubes and p is the pitch (see Fig. 2.1).

The aperture plane passes through the center of the tubes as shown in Fig. 3.4. The length of the aperture plane is taken as the unobstructed length of the collector tubes.

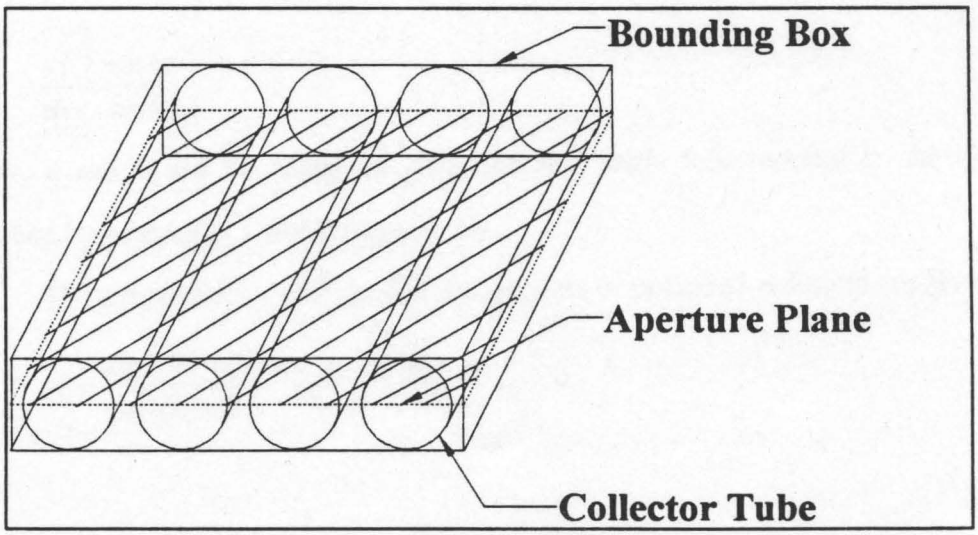

Figure 3.4 Bounding Box and Collector Aperture Plane

The generation of incoming photons or rays is done using either of the methods presented in Section 2.3. Each individual ray is only considered a "ray of interest" if it intersects the bounding box, in which case it is traced further. The ray is in the form of a parametric line and is allowed to pass through the collector model defined in a *binary tree* structure (described in the next chapter) so that its intersection (if any) with all the surfaces of the solid objects making up the collector can be computed. It is possible that some of the incoming rays do not intersect any solid objects or the collector aperture plane and are therefore not of interest in the simulation.

An appropriate algorithm is used to determine the first intersection point of interest, i.e., one which actually exists after the solid combination operations (union, difference or intersection) have been performed. This intersection point will be on one of the different surfaces discussed in Section 2.4. In the following section the fate of an individual ray after intersection with each of these surfaces is discussed.

3.3.1 Intersection with a Transparent Surface

If material encountered by the ray is a transparent one (e.g. glass), the photon may either be refracted or reflected. Refraction occurs in accordance with Snell's law, given by:

$$\frac{n_1}{n_2} = \frac{\sin\theta_2}{\sin\theta_1} \tag{3.3}$$

where, n and θ are the index of refraction and angle from normal in the two media specified by subscripts 1 and 2 respectively.

The perpendicular and parallel components of polarized radiation are given by:

$$r_\perp = \frac{\sin^2(\theta_2 - \theta_1)}{\sin^2(\theta_2 + \theta_1)} \tag{3.4}$$

and,

$$r_\parallel = \frac{\tan^2(\theta_2 - \theta_1)}{\tan^2(\theta_2 + \theta_1)} \tag{3.5}$$

The probability of the reflection is taken as the average of the two components,

$$P_{\text{reflection}} = \frac{1}{2}(r_\perp + r_\parallel) \tag{3.6}$$

Averaging the properties as above is adequate for unpolarized incident radiation, provided there are a small average number of reflections before eventual absorption. This should be a good approximation for this geometry and incident beam radiation. This may not be a good approximation for diffuse radiation, particularly near sunrise and sunset. However, the incident solar is weak at these times, and of little import to determining overall performance. Indeed, the systems will typically not be operated during these times.

The effects of polarization of the light are also accounted for by Knappmiller. The light from the sun is considered unpolarized, and hence at the first intersection with any surface, the effects of polarization do not need to be calculated. However, each subsequent interaction is weighted by the fractions of energy contained in the perpendicular and parallel components of the ray. Perpendicular and parallel components are treated separately to calculate the probability of reflection for each subsequent intersection with any surface. Polarization is thus treated as a statistical function.

The properties needed to be specified for a transmissive surface are its absorptivity and its index of refraction. A perfectly transmissive surface can be defined by setting the absorptivity to zero and the index of refraction to unity.

3.3.2 Intersection with an Opaque Surface

An opaque surface will either be a reflector or an absorber. A reflector will have a certain absorptivity and reflectivity (which can be partially specular and partially diffuse) associated with it. Ideal surfaces, such as perfect reflectors can be specified by setting the absorptivity of the material to zero. On the other hand if the user wants to model a collector without a back plane reflector and the data file already has the reflector defined as part of the geometry, the absorptivity of the material can be set to unity and therefore reflected rays are not possible.

A ray which is reflected specularly leaves the surface in the same plane as that of the incoming ray and the surface normal, and the angle between the rays and the normal are identical and opposite. For diffuse reflection, the departing ray is released at a random angle and direction by assuming an isotropic distribution. In general though, the probability for reflection at an angle θ is proportional to $\cos^r\theta$. The isotropic distribution assumption for θ would correspond to the a value of r equal to zero. For metals, r is usually less than 1 and for nonmetals, r is usually greater than 1 (Maltby, et al. [1994]). The isotropic distribution assumption is a simplification and the code is currently being modified to account for the cosine power dependence. The decision regarding whether the ray is reflected or absorbed is made by generating a random number and a comparison is made between the absorptivity of the reflector and this random number, i.e., if the random number ($0 \leq Rn \leq 1$) is less than the absorptivity of the material, then the ray is absorbed, otherwise it is reflected. If it is reflected, then a second random number is generated to decide whether this reflection is specular or diffuse. Upon a diffuse reflection two outgoing angles are randomly selected from the diffuse directional distribution.

If the surface encountered by the ray is specified as an absorber, then it is the surface within the collector geometry which is intended to absorb the solar radiation. Recall that the $\tau\alpha$ product for a given angle of incidence, as was defined by Equation (2.1), is the ratio of the number of rays absorbed by the collector to the number of rays hitting the collector aperture plane. If the photon after hitting the absorber is absorbed, then the numerator of the fraction in Equation (2.1) is incremented. The denominator of the fraction is incremented when a ray intersects the collector aperture plane on its downward trajectory into the collector geometry as seen from above. Specifically, if a ray happens to get reflected by a back plane without having intersected the aperture plane earlier on, and then intersects the aperture plane on its way up, the denominator of the $\tau\alpha$ fraction would not be incremented. Further, if such a ray were eventually to be absorbed, then only the numerator of the $\tau\alpha$ fraction would be incremented. In this way after all the all the rays have been traced, the final $\tau\alpha$ fraction is determined.

It is possible that after hitting an absorber, the ray is reflected. The probability of this ray getting absorbed later for the geometries considered is assumed to be insignificant. Hence, such a photon would not be traced any further. The program can be modified if such a factor is potentially significant.

Thus the fate of a ray when it intersects various surfaces is determined. From each point of intersection, it may be recast on a new heading or be terminated. If a ray is recast as a new ray, it is again passed through the binary tree to determine new intersections. The first intersection is computed again and the fate of the ray is determined again. The process repeats until all rays have been cast and their outcomes determined.

If a ray passes through a transmissive material, then it may be absorbed before it gets to a new surface. This is determined by calculating the path length within the material and comparing it against the absorptivity per unit distance of material which, as mentioned earlier, has been specified as a property of the material. This kind of treatment of absorption within a transmissive material is okay for "optically thin" materials (Modest,

[1993]), and it is assumed that all cover materials used in solar collectors are optically thin. A ray which is absorbed in such a fashion is terminated.

The ray tracing procedure outlined above is continued until a ray gets absorbed, leaves the collector bounding box or until a maximum number of interactions has been approached. It is necessary to specify a maximum number of interactions to prevent the ray from being caught in an infinite reflective or refractive loop. This maximum number of interactions however will never be reached if the physical properties of the materials are set to realistic values, and the maximum number of reflections is set sufficiently high.

CHAPTER FOUR

MODELING SCHEME

4.1 Requirements

In order to be able to use the Monte Carlo method to determine the optical performance of a solar collector, it is first necessary to define the geometry and material properties of the solar collector in a manner that the computer can store and understand. An appropriate modeling technique must therefore be used so that the collector geometry, however complex it may be, can be represented accurately and without an unreasonable amount of effort on the part of the user.

There are three common techniques which may be used to represent an object in three dimensions, viz., *wireframe*, *surface* and *solid* modeling. Unlike wireframe and surface models, which contain only geometric data, solid models contain both geometric and topological information of the corresponding objects. Geometry consists of the actual dimensions or points which define entities of the object. Topology on the other hand, is the connectivity and associativity of the object entities. In order that informationally complete, valid and unambiguous representation of a solar collector geometry be possible, it is necessary to use a *solid modeling* technique, and the particular technique used here is called Constructive Solid Geometry or CSG.

Once the geometry of the collector has been defined, it is necessary to be able to visualize this geometry so that the user may verify its correctness. Various methods are available for image synthesis on a computer screen and the one used here is called ray tracing (also called *ray casting*). Ray tracing (not to be confused with the ray tracing that

is part of the Monte Carlo simulation), combined with CSG, provides a relatively straightforward way of generating and visualizing 3-D objects on a computer screen.

4.2 Constructive Solid Geometry (CSG)

A CSG model is based on the topological notion that a physical object can be divided into a set of primitives (basic elements or shapes) which can be combined in a certain order following a set of rules (Boolean set operations) to form the object. The program used in this thesis offers the user five different primitives with which to build more complex objects. These are:

- Sphere
- Cone
- Block
- Cylinder
- Cylindrical Paraboloid

These primitives are based on the four *natural quadrics* (since they are the result of basic machining processes): planes, cylinders, cones, and spheres. For example, the block is formed by intersecting six planes. In turn, there are three Boolean set operations that the user can employ to combine any two or more of the primitives listed above:

- Union
- Difference
- Intersection

A hollow tube, for example, is generated by differencing one cylinder from another of a larger diameter. Fig. 4.1, from Roth [1982], shows how a solid object is formed using CSG. The data structure used is based on the concept of *binary trees*. The bottom nodes in the tree are comprised of primitives and all the nodes above are a combination of the nodes below them. Primitives may also make up higher nodes, e.g., where a primitive may be combined with a composite which in turn is comprised of two other primitives.

For computational efficiency, it is best that, wherever possible, the user create a "balanced" tree, i.e., one where the number of nodes and branches are equally distributed to the left and right hand side of the top-most node.

Before primitives can be combined to form composite objects, it is first necessary to size each primitive to the required dimensions and then position it correctly in space. This is done with three *transformation* operators:

- rotation
- scaling
- translation

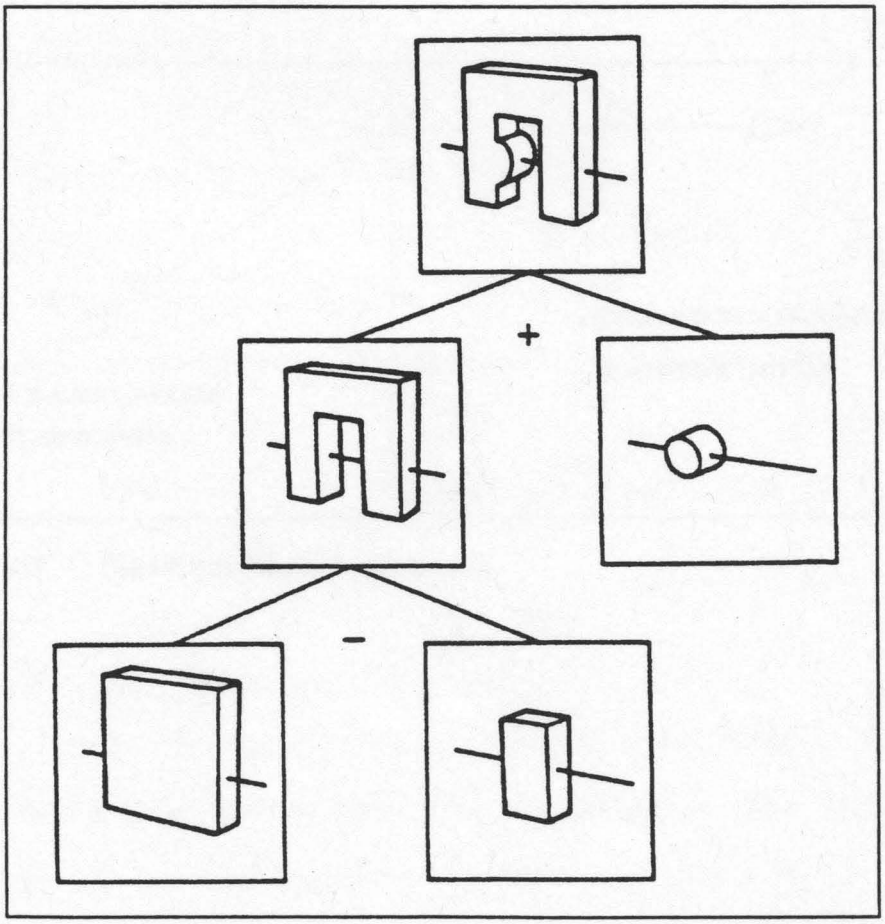

Figure 4.1 Example of Solid Construction Using CSG (From Roth)

Transformations on objects are made with respect to a fixed coordinate system. The coordinate system used in this thesis is a *left-handed* coordinate system. The center of the coordinate system (0,0,0) is located at the center of the computer screen (from the user's point of view). Fig. 4.2 shows how the axes are oriented, and the positive direction of translation and rotation. The positive Z axis points towards the user (i.e., out of the page or screen), while the positive X and Y axes point towards the right and bottom of the page or screen respectively. Positive rotations are identified by pointing the thumb of the left hand in the direction of the coordinate, and curling the fingers of the left hand in the positive direction of rotation inward toward the left palm.

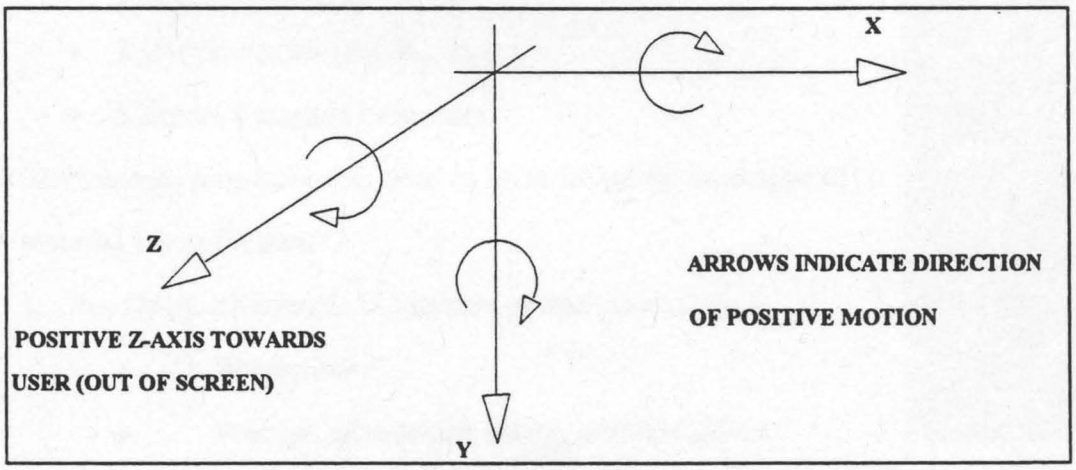

Figure 4.2 User Coordinate System

A sample data file is shown in Text Box 4.1.

```
0 10
-0.5 3.0 -0.5
63.0 0.3 201.6
90 0 0
0 0.04 1.526

0 20
-0.5 -2.0 -0.5
63.0 0.5 201.6
90 0 0
1 0.91 0

0 0
-0.5 -0.5 -0.5
63.0 2.2 201.8
90 0 0
0 0 0

0 101
-0.5 -0.5 -0.5
63.0 0.1 201.0
90 0 0
0 0 0

9 0

0 99 10 20

9 0 0 0
```

4.1 Sample Data File

The data file contains all the relevant information regarding each primitive as well as a *connectivity array* that specifies the way in which the primitives are combined using the Boolean operations (i.e., type of operations used and order in which they occur).

Information regarding the primitives appears sequentially, line by line, and includes:

- Primitive Type and Number
- Translation Coordinates (T_X, T_Y, T_Z)
- Scaling Values (S_X, S_Y, S_Z)
- Rotation Angles (R_X, R_Y, R_Z)
- Material Type and Properties

The material properties that need to be specified for each type of material are as follows:

1. For Opaque Materials (Absorbers or Reflectors):
    - Absorptivity
    - Fraction of reflected energy which is diffuse
2. For Transmissive Materials (Glass, etc.):
    - Absorptivity per thickness of material
    - Index of refraction in solar spectrum

The data file in Text Box 4.1 consists of two primitives (blocks that are numbered 10 and 20), that are combined to form the final composite (numbered 99). In addition to these two primitives, two other objects are defined in the data file. These are the bounding box (numbered 0) and the aperture plane (numbered 101) which are both defined in the previous chapter. These objects do not appear in the connectivity array as

they are not a physical part of the collector geometry. They are used only for the Monte Carlo simulation.

The generation of a data file can be a fairly time consuming process, especially if the collector geometry is involved. However, once the binary tree has been created, the conversion to numerical values in the data file is a relatively straightforward and logical process.

CHAPTER FIVE

IMPLEMENTATION

5.1 Platforms Used

The software used in this thesis can be separated into the following two routines:

- Display Routine
- Monte Carlo Routine

The display routine is the one used to generate the input file and graphically display the collector geometry so that it can be verified by the user. The programs associated with this routine are executed on an IBM compatible PC using the Borland Turbo C 2.0 compiler. Color images of the collector geometry are displayed in color VGA mode.

Once the geometry has been verified, the input file (without any modification in format, etc.) is passed to the Monte Carlo routine. The Monte Carlo simulation may be run on an IBM compatible PC or a UNIX operating system based workstation. Execution of the Monte Carlo code on a PC though, takes a very long time, and thus the code is usually run on DEC 2000, 3100 and 5000 workstations (all UNIX based) which are part of the Local Area Network for the College of Engineering (LANCE). The problem of casting multiple rays, all needing to be executed using the same program and same geometry, is very suitable for distributed computing. Hence a distributed system implementation is used to spread the computing load over many workstations, thereby dramatically reducing overall computation time. This implementation is described in the following section.

5.2 Distributed System Implementation

As discussed in Section 2.3, the input to the program consists of the X, Y and Z coordinates of the tail points for the input vectors which in effect specify the direction of incoming radiation. Using the input vector distribution shown in Fig. 2.3 requires a total of 324 input vector origins. Tracing the rays from all the different angles of incidence on a single workstation would require a prohibitive amount of time as each direction of incoming radiation corresponds to thousands of photons that need to be cast and traced to extinction.

A distributed system implementation wherein many input vectors were run concurrently on different workstations was used by Knappmiller. This implementation is based on shell script programs which search the network for computers which are not in active use, and then load on each available machine the program executable file with an appropriate vector as command line input. The results from each machine are then concatenated into a single output file. However, the number of machines available is almost always far fewer than the number of input vectors, and hence the process of seeking out new machines and loading the files needs to be repeated manually until all the input vectors have been loaded in succession. The process was improved marginally by the automation of the break up of the original input vector list into smaller lists based on the number of machines available, but the subsequent loading of the executable file and command line input on each available machine was still done manually. The user had to wait until results from all the vector inputs from one batch are obtained before the next batch could be sent for execution. This process is prone to many problems, the most common being workstations "crashing" during program execution. This can result in significant delays as all batch files must wait for the results from all machines before they can return a completed set of results.

Dempsey [1992] developed a technique that would permit the user to describe a job stream and instruct the system to execute those jobs using the best combination of

resources available. The user describes a job in terms of a job identifier, a resource requirement (e.g. machine architecture such as vax, mips, etc.), a dependency indicating which jobs may run concurrently (mapping of a precedence graph), the job itself as a shell command, the limits on required number of nodes (individual machines within the network) and the acceptable load on each node. All this is done with help of a job control file.

Once the job control file is created, the user simply follows a specified list of commands to initiate the distributed processing. Available nodes are sought out and the first set of input vectors (corresponding to the number of machines available) are processed with the remaining vectors queuing up and ready to go. A new vector is processed as soon as a machine becomes available. Successful processing of each vector may not occur in the same order as it was initiated, as the load on each machine may vary. However, each vector has an identifier, and the final output file consists of all the results appropriately ordered. In the event that a process fails due to software errors, etc., the queue is not held up and the next vector is processed as soon as possible. This continues until all vectors have been processed. In addition to the output file, a "progress status" is constantly updated, informing the user of completed jobs as well as any jobs that may terminate unsuccessfully.

Instructions and other relevant notes regarding the actual implementation procedure are included in Appendix A.

5.3 Modifications to Previous Version of Code

The following modifications were made to the existing version of the computer code developed by Knappmiller:

5.3.1 Absorption within a Reflector

A realistic reflective surface within a collector's geometry will have a certain amount of absorptivity associated with it. Therefore, when a ray intersects such a surface, a test must be performed to determine whether absorption occurs. The ray trace must be terminated for a ray that is absorbed by the reflector. This particular test was omitted in the previous version of the code resulting in higher absorbed fractions when analysis with a reflective surface behind the tubes was considered.

The necessary rectification has been made, and the code has been thoroughly tested to ensure that the specified absorptivity of a reflector is accounted for in the calculations.

5.3.2 Order of Transformations in CSG Segment of Code

Section 4.2 describes how a primitive object is defined and positioned in space under the three transformations: rotation, scaling and translation. The order in which these transformations are made yields vastly different results in the final position of an object.

The origin of the coordinate system used is located at the center of the screen and all transformations are made with respect to this origin. The previous version of this code segment was set up first to translate an object, then scale it, and finally rotate it. This order of transformation can be very confusing to the user as the object rotates about the original coordinate system, and therefore, appears to have revolved (in a circular arc) about the origin coordinates. The user would have to account for this and modify the translation values to position the object correctly. It is preferable to rotate the object first, then scale and finally translate it in space, as the object will not revolve about the origin. This modification has been made, and now the positioning of primitives in space before the set operations are performed may be done in an intuitive manner.

5.3.3 Portability to MIPS Architecture

The previous implementation of distributed processing was restricted to running on Vax 2000 workstations at LANCE. Vax 2000 workstations are of the vax architecture, and are considerably slower platforms than the DEC 3100 and 5000 workstations which are of the mips architecture. Running the original code on mips architecture machines resulted in segmentation errors which were traced down to the problem of "NULL" pointers being referenced. This problem has been successfully overcome, and the code now runs on any platform, irrespective of architecture. The programs need to be re-compiled only when a new machine architecture is encountered.

There are currently two versions of the program executable (for vax and mips architectures respectively) available on LANCE, and the distributed system implementation loads the appropriate executable file when a particular architecture is encountered.

CHAPTER SIX

RESULTS

6.1 Parametric Design Study of NEG Sun Family Collector

Results from the parametric design study conducted on the NEG Sun Family solar collector are discussed in this section. The five geometric parameters enumerated in Section 2.2 are varied, and $\tau\alpha$ and IAM values are computed using the Monte Carlo ray tracing program. Although these values of $\tau\alpha$ and IAM are calculated for all of the 324 combinations of γ and β corresponding to the input directions shown in Fig. 2.3, results are presented only for the following eight different combinations of γ and β:

$\beta = 0°, \gamma = 0°, 30°, 50°, 70°$

$\beta = 60°, \gamma = 0°, 30°, 50°, 70°$

The eight combinations of γ and β shown above were used to submit results to the International Energy Agency (IEA), and it is believed that these are the minimum number of data points that can be used to provide a good indication of a collector's optical performance. All calculations were done at a specified accuracy of 1 %.

The base geometry in this study is a single module consisting of four 2 meter long glass tubes, each 12.6 cm in diameter. Inside each tube is a 11.0 cm diameter absorber tube. The four tube module is a total of 63.0 cm wide, corresponding to a tube pitch of 15.8 cm. Fig. 2.1 shows this base geometry.

6.1.1 Effect of Back Plane Reflectance

Intuitively, one would expect the performance of a solar collector to be enhanced as the reflectivity of a back plane is increased. However, it is important to have a quantitative idea of this effect so as to aid in the selection of a reflective surface that is a

compromise between performance and cost. Four different back plane reflectivities were modeled for a four tube collector. The width of the back plane was set at the aperture width of the collector (63.2 cm). Reflectivity values were selected as 0.0 (corresponding to a case where there is no reflector), 0.2, 0.8 and 1.0 (perfect reflector). Reflectivity (ρ_{bp}) was assumed to be 100 % diffuse, i.e., no specular component. The effect of ρ_{bp} on $\tau\alpha$ is shown in Figs. 6.1 and 6.2.

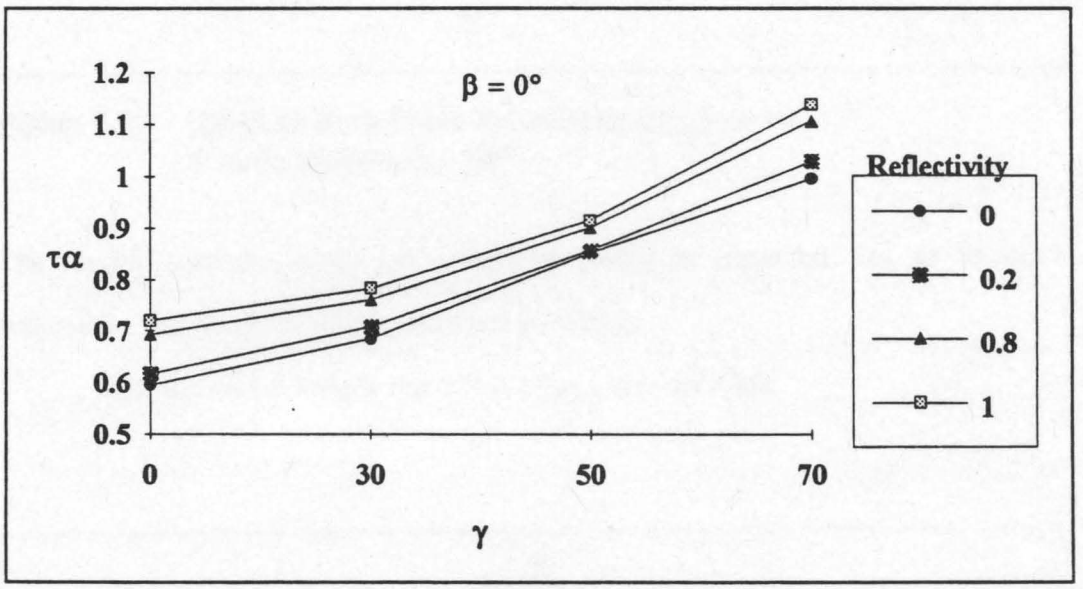

Figure 6.1 Effect of Back Plane Reflectivity (ρ_{bp}) on $\tau\alpha$ 4 Tube Module, $\beta = 0°$

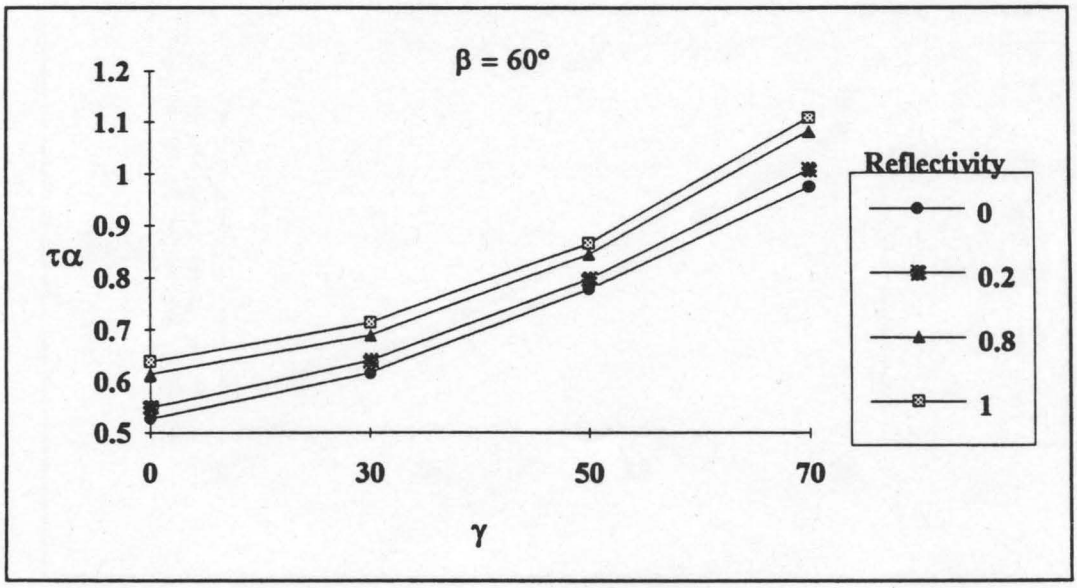

Figure 6.2 Effect of Back Plane Reflectivity (ρ_{bp}) on τα
4 Tube Module, β = 60°

The results from this study are exactly as would be expected, i.e., an increase in the reflectivity will result in higher absorbed fractions.

Figs. 6.3 and 6.4 show the effect of ρ_{bp} on the IAMs.

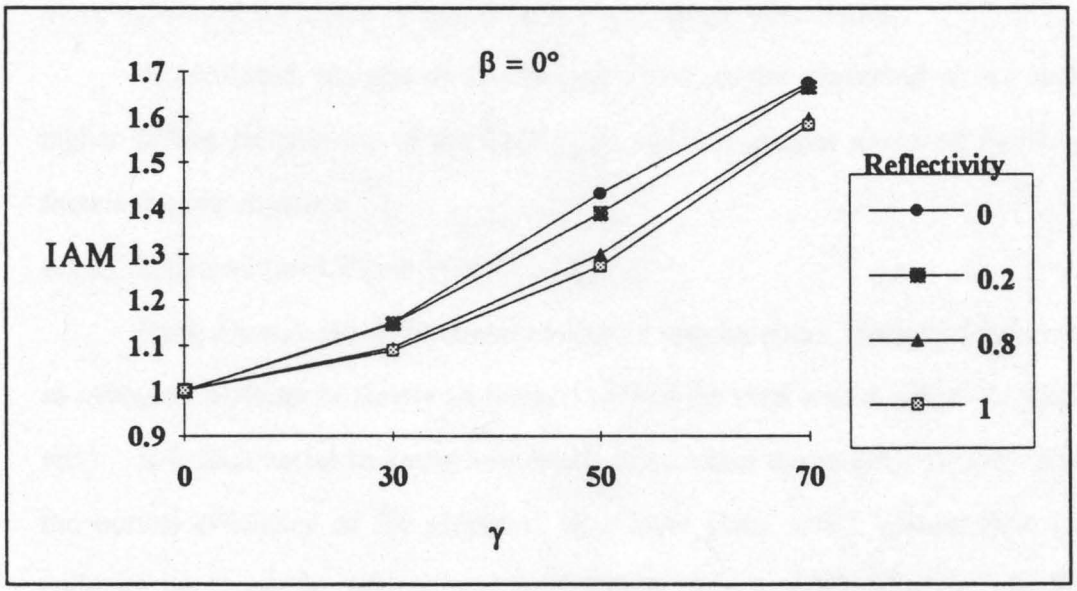

Figure 6.3 Effect of Back Plane Reflectivity (ρ_{bp}) on IAM
4 Tube Module, β = 0°

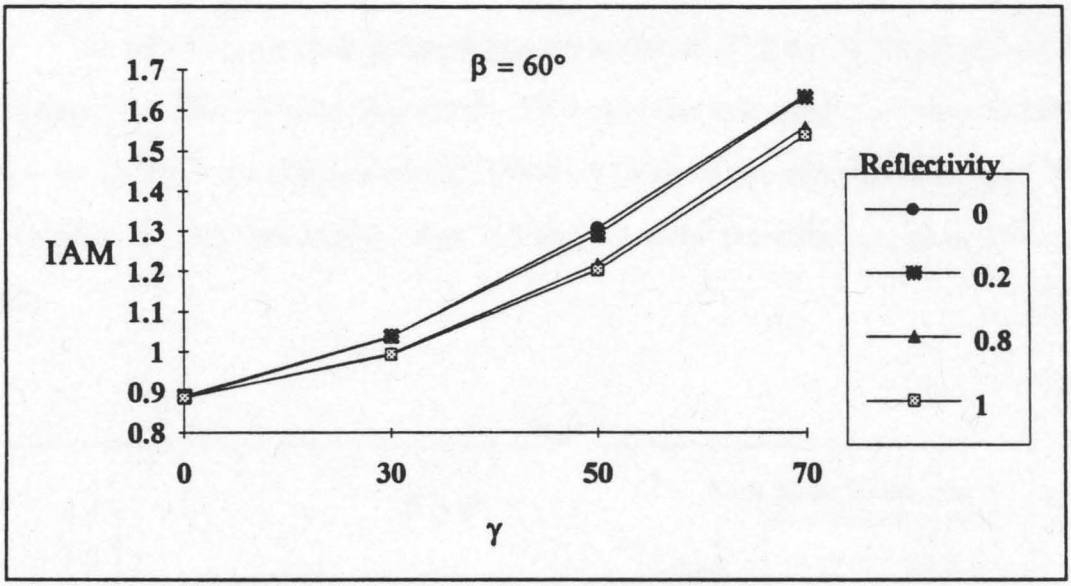

Figure 6.4 Effect of Back Plane Reflectivity (ρ_{bp}) on IAM 4 Tube Module, $\beta = 60°$

The variation in the IAM values is not very significant when the reflectivity of the material is varied. However, the IAMs for lower reflectivities are slightly higher than those for higher reflectivities. This indicates that the amount of back scattering of radiation from the reflector to the tubes at normal incidence compared to off-angle incidence is relatively more significant for higher reflectivities than for lower reflectivities.

A combined analysis of the $\tau\alpha$ and IAM results presented above indicate that higher diffuse reflectivities of the back plane result in greater absorbed fractions and are therefore advantageous.

6.1.2 Effect of Back Plane Width

Back planes used with tubular collectors may be either specially fabricated to serve as reflective surfaces or simply an integral part of the roof with a selective coating (paint, etc.). It is thus useful to know how much of an effect the width of a back plane has on the optical efficiency of the collector, as a back plane width greater than that of the collector itself may be quite easy to incorporate. The length of the back plane is usually the same as that of the collector.

The following six back plane widths are analyzed: 63.2 cm (aperture width), 88.4 cm (aperture width + 2 tube diameters), 113.6 cm (aperture width + 4 tube diameters), 126.4 cm (2 times the aperture width), 189.6 cm (3 times the aperture width) and 316.0 cm (5 times the aperture width). Figs. 6.5 and 6.6 show the effect on $\tau\alpha$ of back plane width.

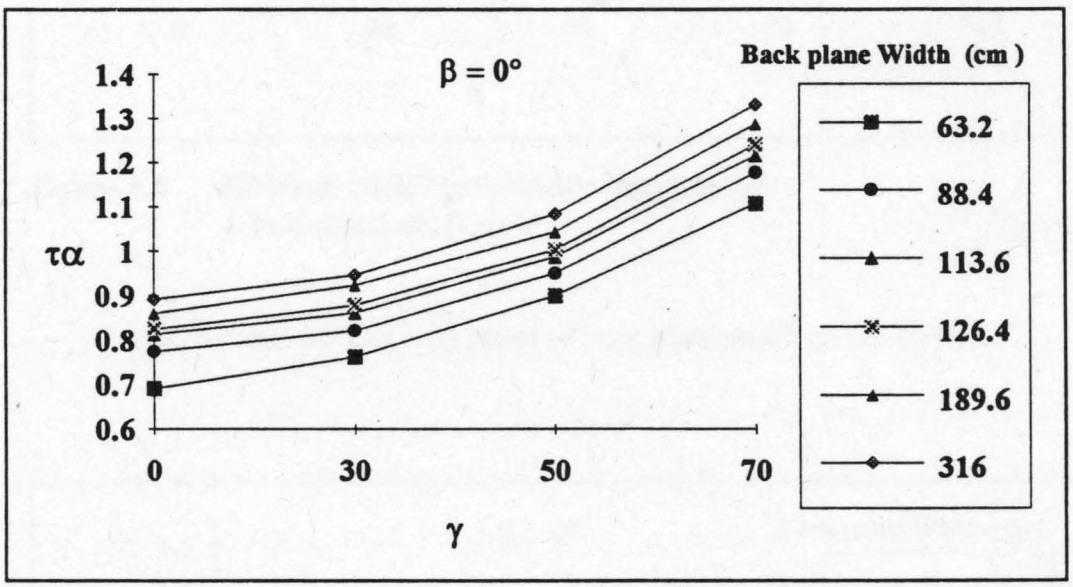

Figure 6.5 Effect of Back Plane Width (bp_W) on $\tau\alpha$ 4 Tube Module, $\beta = 0°$

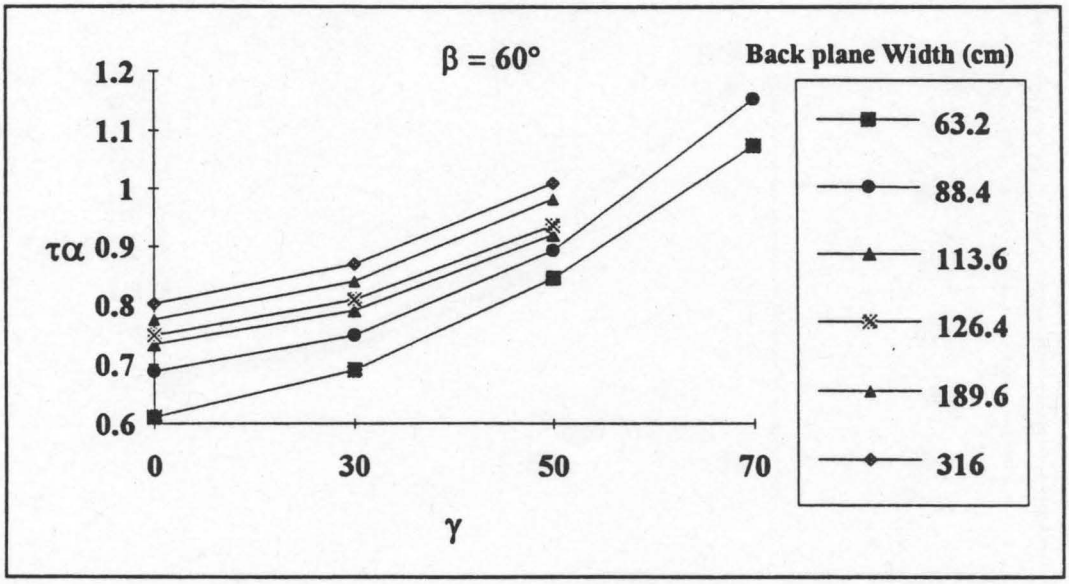

Figure 6.6 Effect of Back Plane Width (bp_W) on τα
4 Tube Module, β = 60°

Figs. 6.7 and 6.8 show the effect of back plane width on the IAMs.

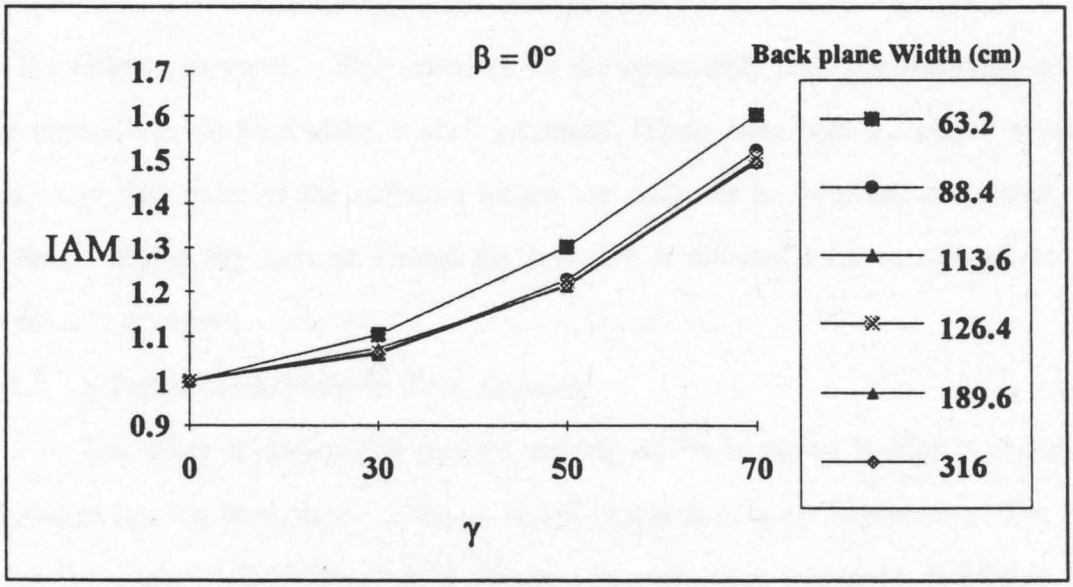

Figure 6.7 Effect of Back Plane Width (bp_W) on IAM
4 Tube Module, β = 0°

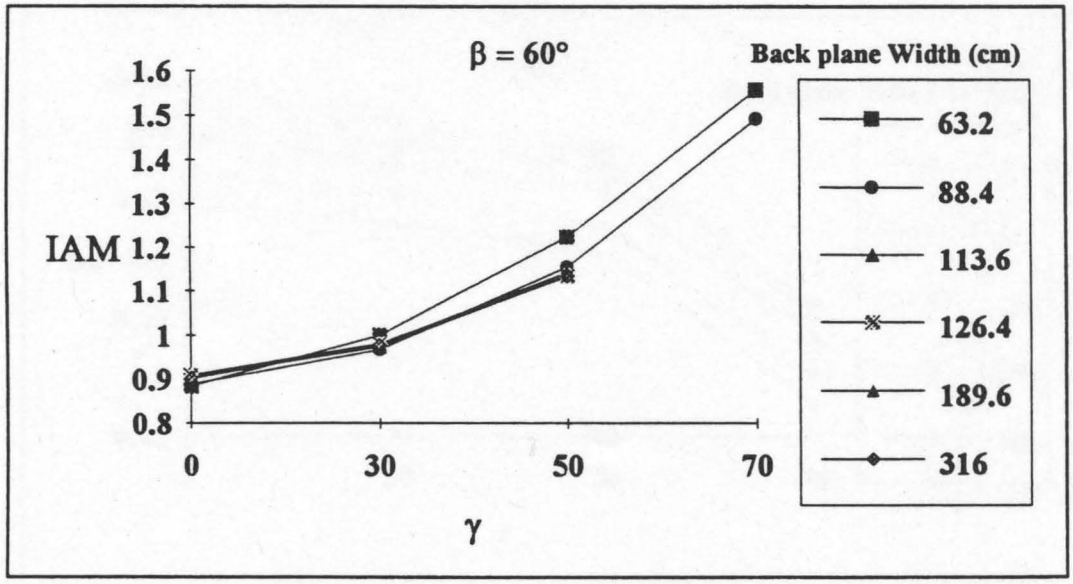

Figure 6.8 Effect of Back Plane Width (bp_W) on IAM 4 Tube Module, β = 60°

The results shown above indicate a significant improvement in the absorbed fraction at various angles of incidence as the width of the back plane is increased. During this analysis the width of the aperture plane is maintained constant at 63.2 cm while the width of the reflector is varied. This accounts for the remarkably high absorbed fractions that are observed as the back plane width is increased. Thus, these high absorbed fractions do not mean that more of the radiation hitting the collector is absorbed, but rather, more radiation hitting the surfaces around the collector is directed back to the collector and eventually absorbed.

6.1.3 Effect of Back Plane to Tube Spacing

The effect of back plane to tube spacing on τα is shown in Figs. 6.9 and 6.10. Optimum spacing between the reflector and the tubes is of great importance. The results from this analysis should be used in conjunction with those presented in Section 6.2 to determine whether it is really necessary to have a reflective surface behind the tubes. Five different values are selected for this analysis. These are 1, 5, 10, 20 and 30 cm, 5 cm being the base case.

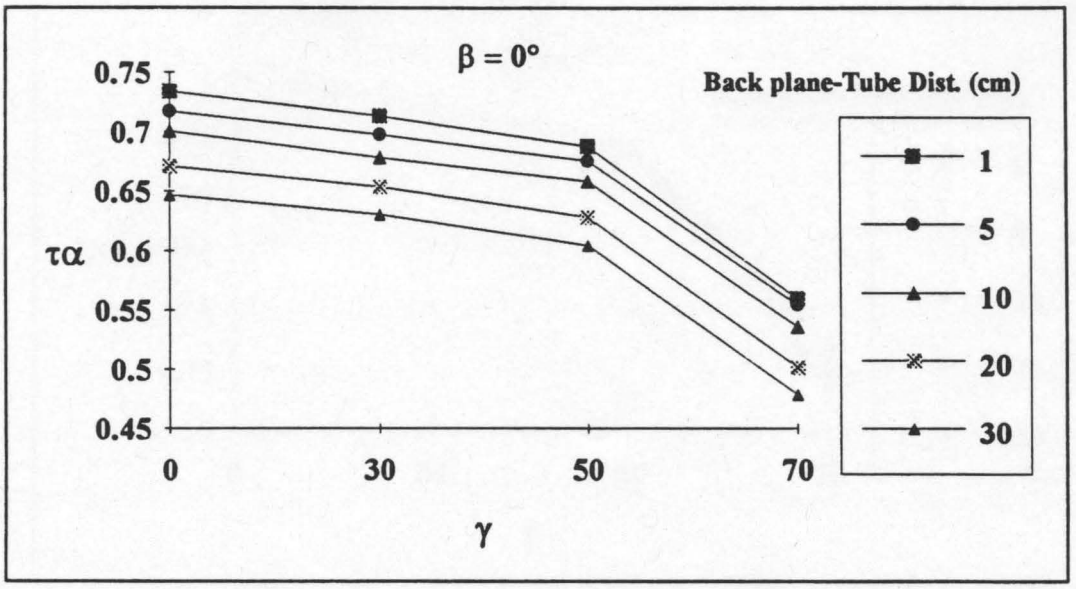

Figure 6.9 Effect of Back Plane-Tube Spacing on τα
4 Tube Module, β = 0°

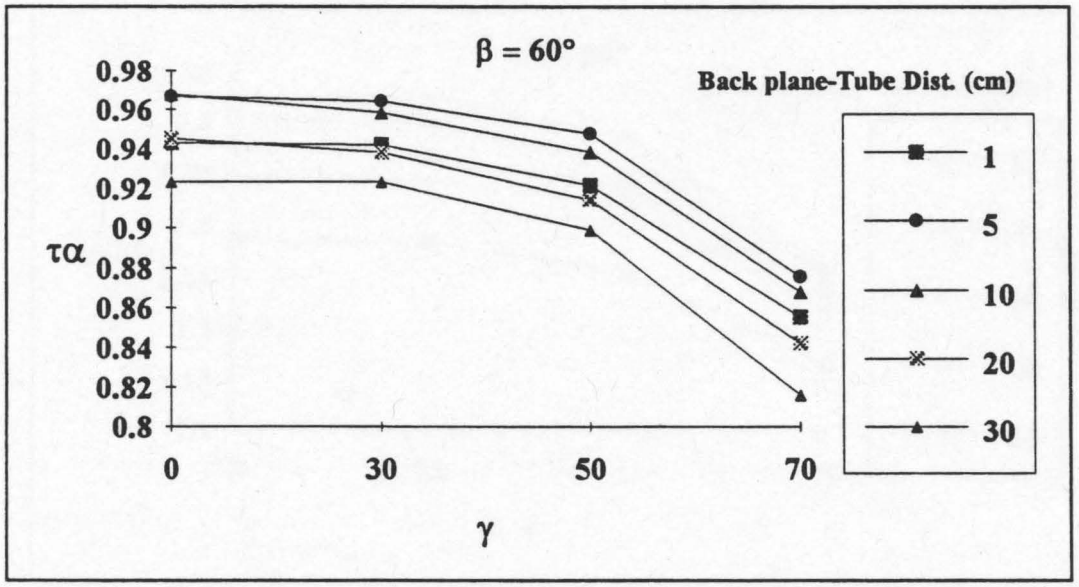

Figure 6.10 Effect of Back Plane-Tube Spacing on τα
4 Tube Module, β = 60°

Figs. 6.11 and 6.12 show the effect various reflector to tube distances have on the IAMs.

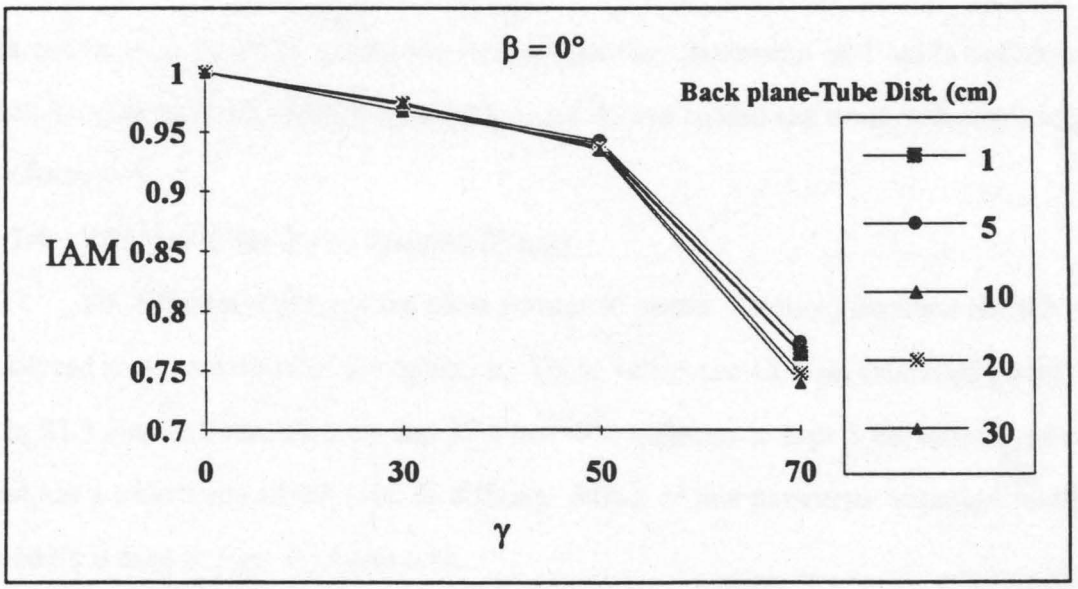

Figure 6.11 Effect of Back Plane-Tube Spacing on IAM 4 Tube Module, β = 0°

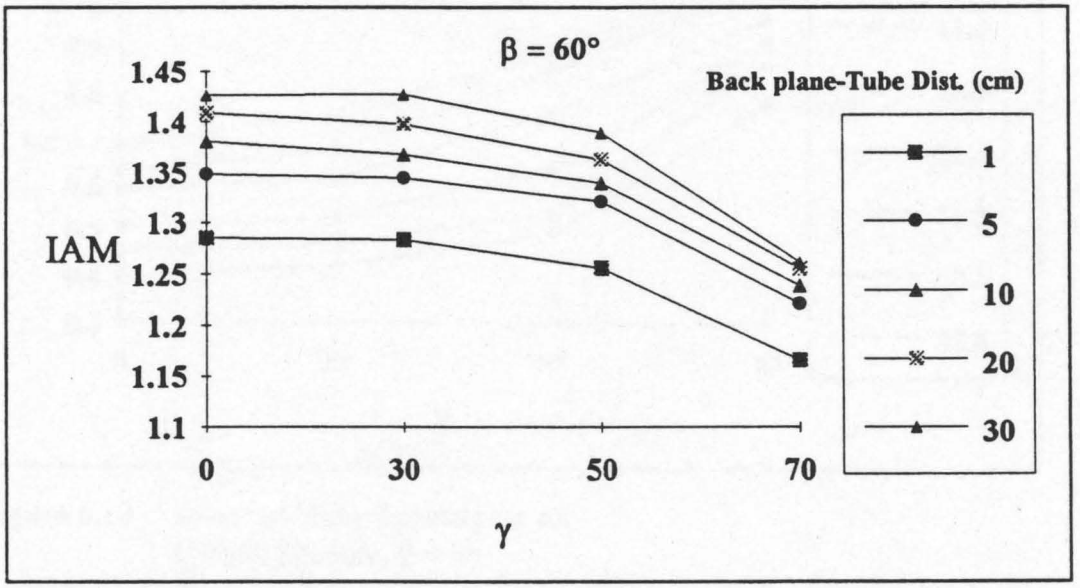

Figure 6.12 Effect of Back Plane-Tube Spacing on IAM 4 Tube Module, β = 60°

As can be seen from the graphs above, the base case dimension of 5 cm is optimum. In fact, keeping the back plane between 5 cm and 10 cm behind the tubes will result in good performance.

6.1.4 Effect of Inter-Tube Spacing (Pitch)

Six different values of the pitch (center to center distance) between the tubes are analyzed so as to determine the optimum. These values are 15.8 cm (standard pitch), 18.6 cm, 21.3 cm, 26.8 cm, 32.3 cm and 37.8 cm. The reflector is kept 5 cm behind the tubes, and has a reflectivity of 0.8 (100 % diffuse). Effect of this parameter variation on the $\tau\alpha$ product is seen in Figs. 6.13 and 6.14.

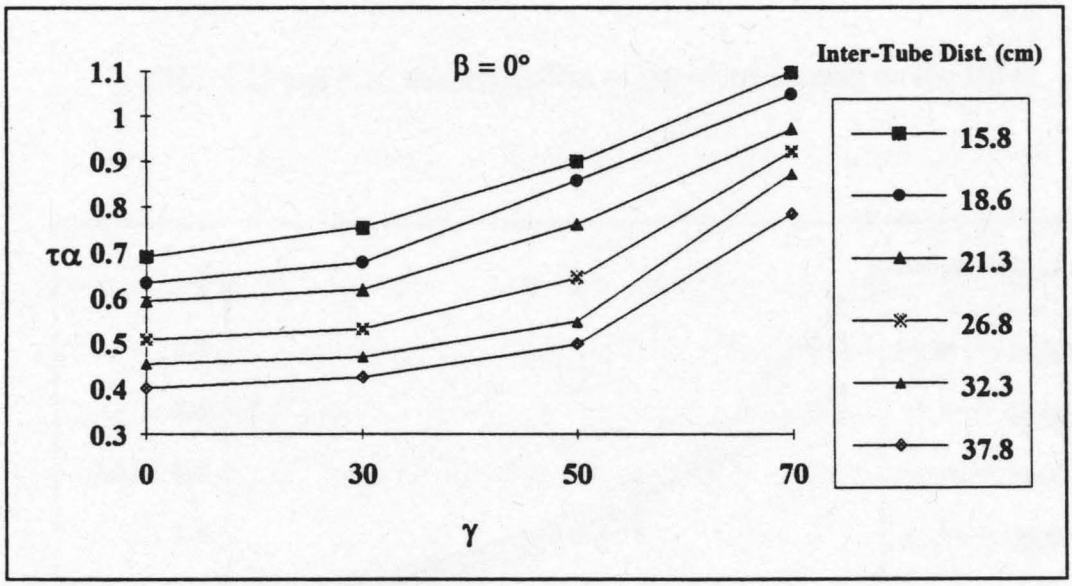

Figure 6.13 Effect of Tube Spacing on $\tau\alpha$
4 Tube Module, $\beta = 0°$

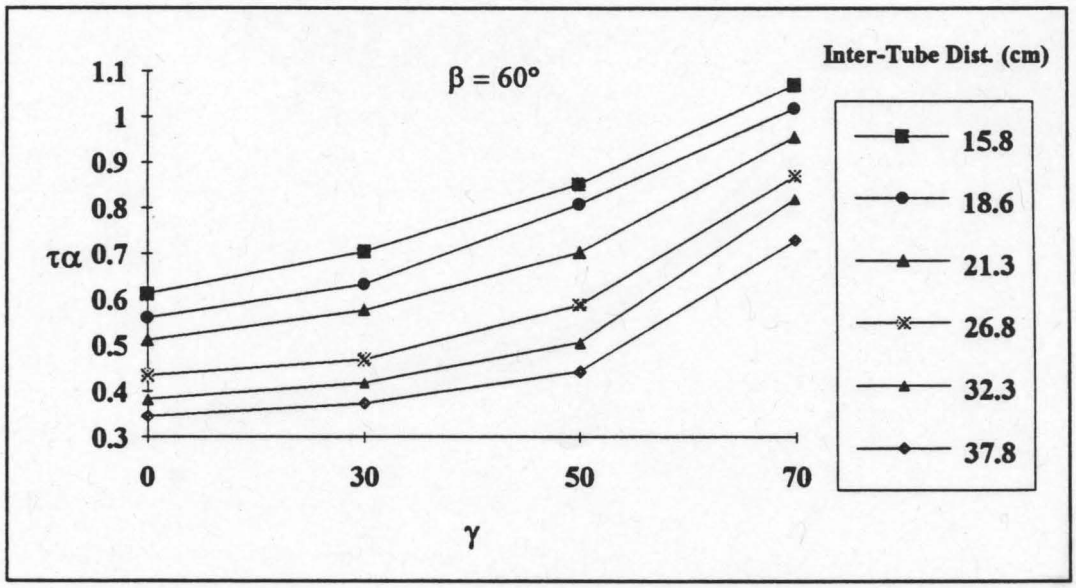

Figure 6.14 Effect of Tube Spacing on τα
4 Tube Module, β = 60°

Figs. 6.15 and 6.16 show the effect of inter-tube spacing on the IAMs.

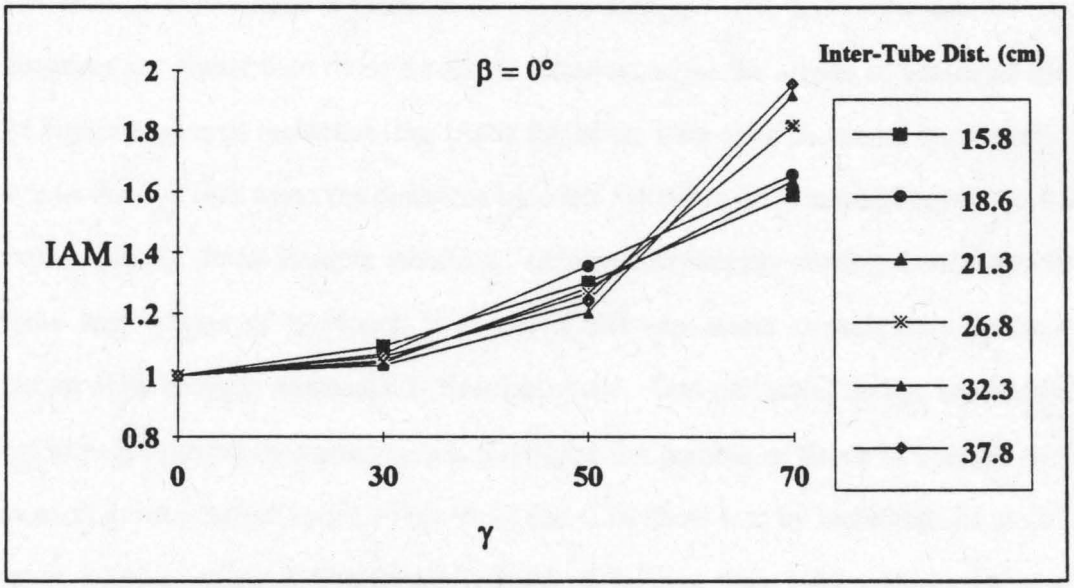

Figure 6.15 Effect of Tube Spacing on IAM
4 Tube Module, β = 0°

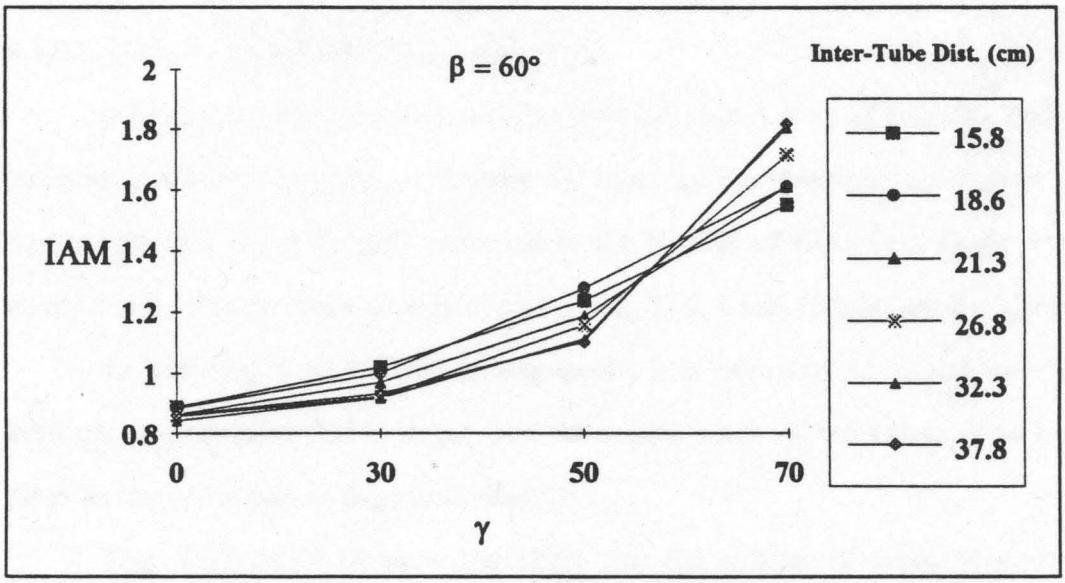

Figure 6.16 Effect of Tube Spacing on IAM
4 Tube Module, β = 60°

The absorbed fractions at all the angles of incidence considered are inversely proportional to the distance between the tubes as is observed in Figs. 6.13 and 6.14. However, the variation in IAMs does not follow the same pattern. The IAMs for smaller inter-tube distances are higher than those for larger distances when the angles of incidence are lower. At higher angles of incidence, the IAMs for larger inter-tube distances are higher. This is due to the fact that when the distances between the tubes is increased, more tube surface is exposed to the direct incident radiation. Although the energy coming from the radiation at these high angles of incidence is lower, it still represents considerable heating power during early daylight hours and is thus beneficial. One particular design modification that has been suggested by researchers is to reduce the number of tubes in a single module by mounting them farther apart. Figs. 6.13 and 6.14 show that by including about 20% more space between tubes, performance is reduced by less than 10%. Increased heat losses aside, this suggests a potentially more cost effective design.

6.1.5 Effect of Number of Tubes / Modules

NEG Sun Family collectors are usually installed in 4, 8 or 12 tube arrangements (4 tubes per module). One design variation discussed by the researchers in this project and the manufacturers is a possible reduction in the number of tubes in a single module to either 2 or 3. The ray trace is carried out for 1, 2, 3, 4, 8 and 12 tube configurations.

In analyzing 8 or 12 tube arrangements, it is necessary to model the extra gap between two modules that is larger than the regular pitch of the tubes. This extra gap plays an important part in edge tube effects.

Figs. 6.17 and 6.18 show the effect that the number of tubes have on the $\tau\alpha$ product.

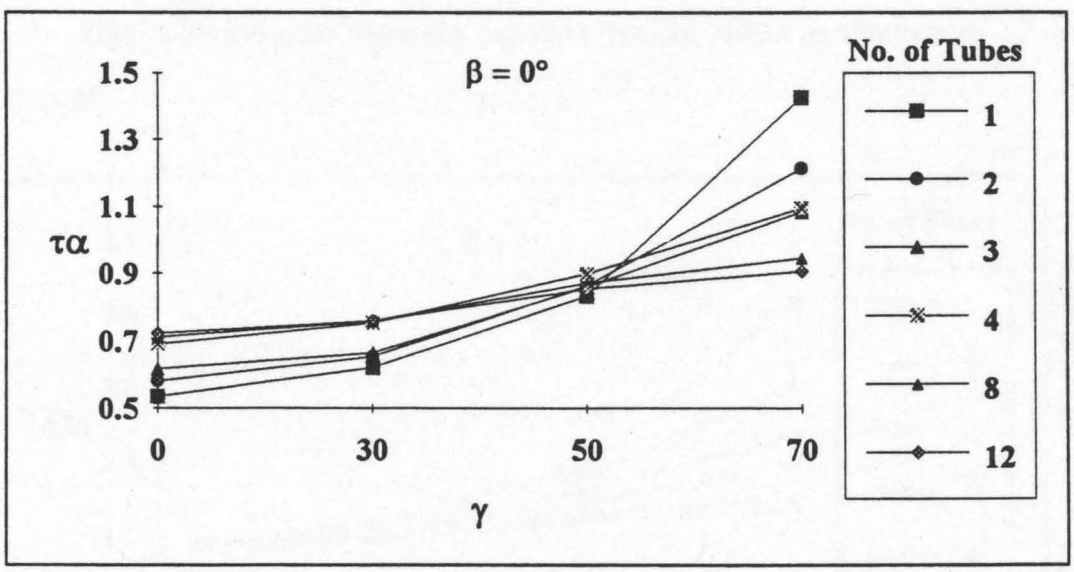

Figure 6.17 Effect of Number of Tubes on $\tau\alpha$
$\beta = 0°$

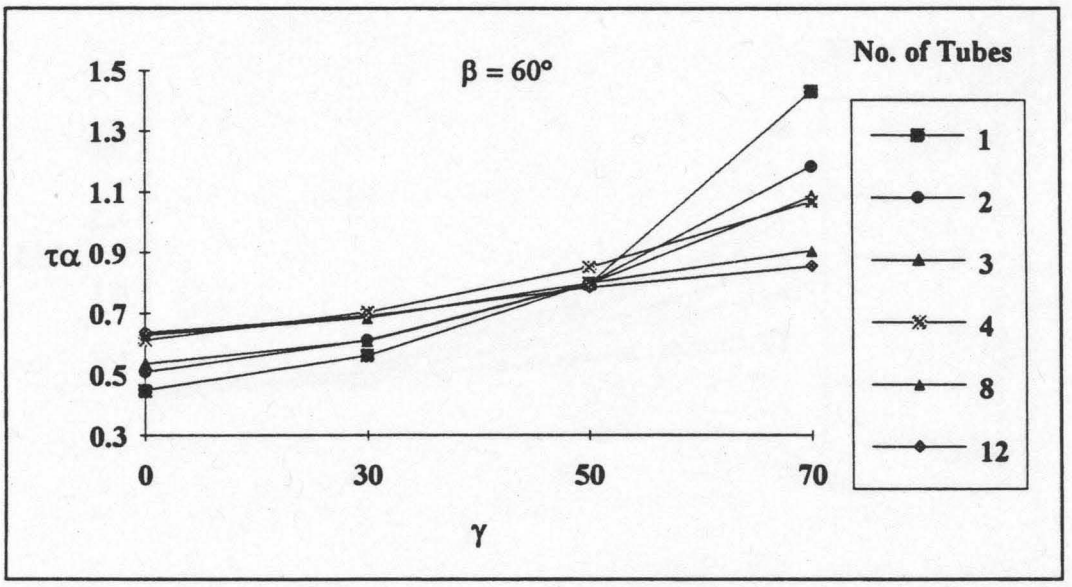

Figure 6.18 Effect of Number of Tubes on τα
β = 60°

Figs. 6.19 and 6.20 show the variation in IAM values as the number of tubes is increased.

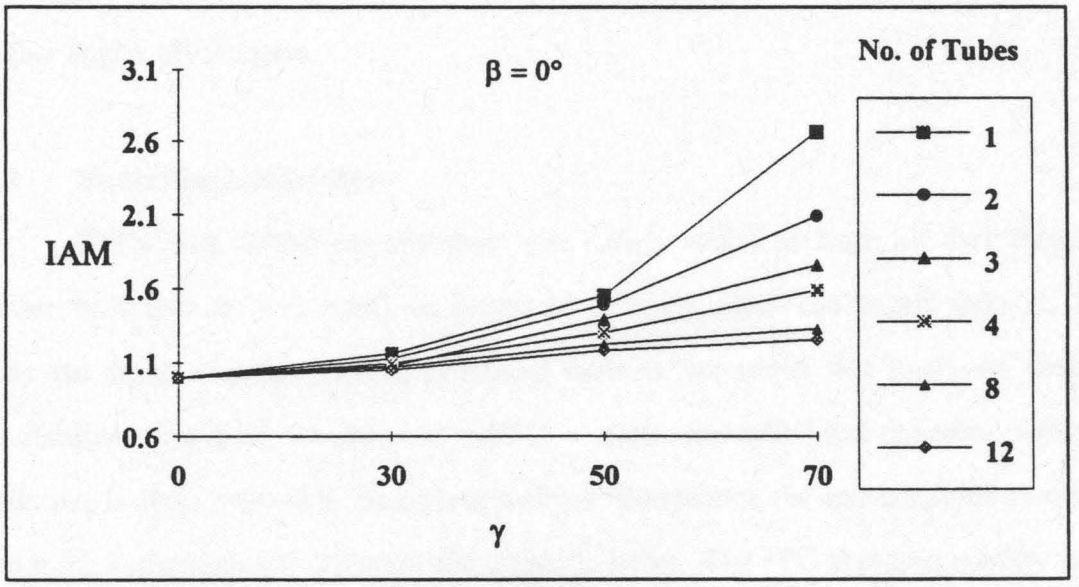

Figure 6.19 Effect of Number of Tubes on IAM
β = 0°

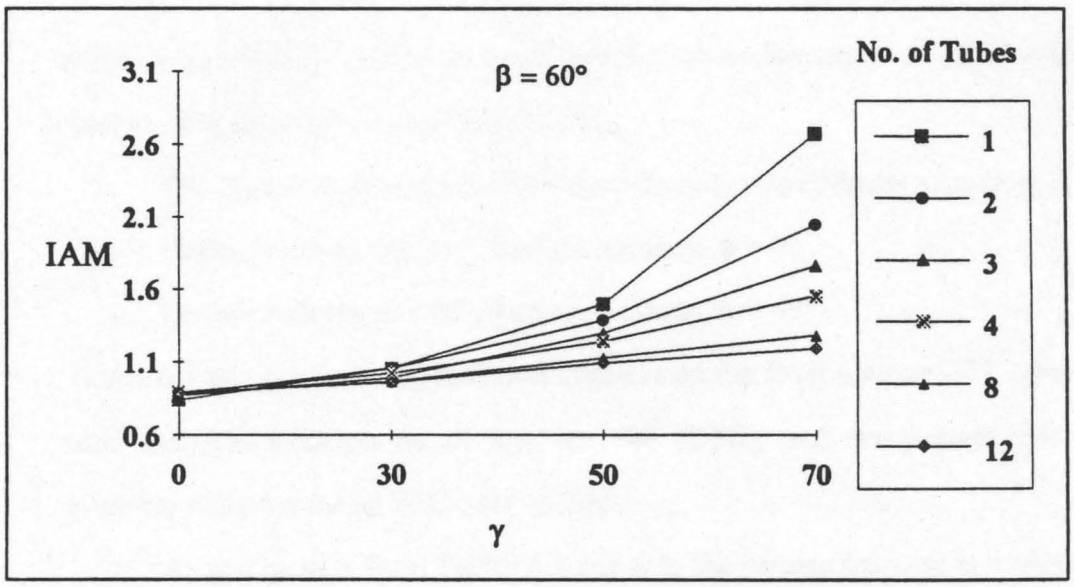

Figure 6.20 Effect of Number of Tubes on IAM
β = 60°

At lower angles of incidence fewer tube numbers correspond to lower absorbed fractions, but this trend gets reversed at higher angles of incidence. This is because the amount of shading due to adjacent tubes gets reduced as the total number of tubes in a module decreases. Consequently, the IAMs for fewer number of tubes are significantly higher at higher angles of incidence.

6.2 Radiation Availability

ETCs with cylindrical absorbers can collect radiation from all four directions (front, back and the two sides), as compared to FPCs which can collect radiation from only the front. In the method presented here to determine this increased radiation availability of an ETC compared to a FPC, a multi-tube cylindrical collector, without a reflector, is approximated by four plane surfaces representing the active collection areas of the front, back and sides of the tubular collector array. The FPC is represented by its one active surface.

Radiation available to each surface is determined for four cities (Madison, Miami, Sacramento and Fresno) using the Klein-Theilacker (K-T) [1981] method. This model

assumes that both sky and ground diffuse radiation are isotropic. A monthly calculation is used to determine the average daily effects.

The analysis was performed for the following two collector orientations:

- Collector Slope, $\beta = 60°$, Surface Azimuth, $\phi = 0°$
- Collector Slope, $\beta = 60°$, Surface Azimuth, $\phi = 45°$

Tables 6.1 and 6.2 show the radiation available on the front surface (FPC), the sum of the total radiation available on all four surfaces (ETC), and the percent (%) increase in available radiation for an ETC over an FPC.

As can be seen from Tables 6.1 and 6.2, the percent increase in available radiation is as high as 89% during the months of April through August, and is at least higher than 33% during the months of September through March.

ICS-ETC modeled as a 4-sided box (4 active surfaces)
FPC modeled as the front surface of the 4-sided box (1 active surface)
Collector slope = 60°, surface azimuth = 0°

	Front Surface (FPC)				**All 4 Surfaces (ETC)**				**% increase in available radiation**			
	HT (MJ/m^2)				HT (MJ/m^2)							
	Mad.	**Mia.**	**Sac.**	**Fres.**	**Mad.**	**Mia.**	**Sac.**	**Fres.**	**Mad.**	**Mia.**	**Sac.**	**Fres.**
Jan	10.7	15.9	10.7	11.4	14.3	22.4	14.7	15.8	**33.7**	**41.1**	**37.8**	**38.4**
Feb	13.9	16.7	14.9	15.7	19.2	24.8	20.9	22.1	**38.6**	**48.1**	**40.8**	**41.0**
Mar	15.0	17.0	18.8	19.9	22.4	26.6	27.8	29.4	**48.9**	**56.5**	**48.0**	**47.9**
Apr	14.7	16.0	20.5	21.0	23.7	27.1	32.5	33.3	**61.1**	**69.0**	**58.5**	**59.0**
May	15.8	13.6	20.6	20.4	27.2	24.9	35.4	35.3	**71.4**	**82.9**	**71.9**	**72.9**
Jun	16.5	12.1	20.5	20.3	29.3	22.8	37.0	36.9	**77.6**	**89.3**	**80.4**	**81.9**
Jul	16.9	12.7	21.4	20.8	29.4	23.7	37.6	36.9	**74.5**	**86.5**	**76.2**	**77.5**
Aug	17.0	13.3	22.4	22.3	27.8	23.4	36.3	36.4	**63.8**	**75.4**	**62.3**	**63.2**
Sep	15.7	14.1	23.1	23.5	24.0	23.1	34.3	35.0	**52.7**	**63.3**	**48.7**	**49.3**
Oct	14.5	15.4	20.4	21.8	20.5	23.5	28.6	30.5	**41.1**	**52.2**	**40.2**	**40.1**
Nov	9.2	16.2	14.5	16.4	12.7	23.0	19.6	22.1	**38.2**	**42.6**	**35.5**	**35.0**
Dec	7.8	16.2	10.2	10.3	10.6	22.5	13.9	14.2	**35.5**	**39.0**	**35.9**	**37.6**

Analysis done on monthly basis for Madison, Miami, Sacramento and Fresno

Table 6.1 ETC - FPC Comparison ($\beta = 60°$, $\phi = 0°$)

ICS-ETC modeled as a 4-sided box (4 active surfaces)
FPC modeled as the front surface of the 4-sided box (1 active surface)
Collector slope = 60°, surface azimuth = 45°

	Front Surface (FPC)				**All 4 Surfaces (ETC)**				**% increase in available radiation**			
	HT (MJ/m^2)				HT (MJ/m^2)							
	Mad.	**Mia.**	**Sac.**	**Fres.**	**Mad.**	**Mia.**	**Sac.**	**Fres.**	**Mad.**	**Mia.**	**Sac.**	**Fres.**
Jan	8.8	13.7	9.0	9.6	12.8	20.6	13.4	14.4	**46.1**	**49.8**	**49.1**	**49.2**
Feb	11.8	15.1	12.8	13.6	17.6	23.4	19.3	20.4	**49.2**	**55.2**	**50.5**	**50.3**
Mar	13.6	16.3	17.2	18.3	21.4	26.2	26.8	28.4	**57.2**	**61.2**	**55.9**	**55.5**
Apr	14.3	16.6	20.3	20.9	23.8	28.1	33.2	34.2	**66.1**	**69.9**	**63.3**	**63.4**
May	16.2	14.9	21.9	21.9	28.0	26.7	37.5	37.7	**72.7**	**78.9**	**71.7**	**72.1**
Jun	17.3	13.4	22.7	22.6	30.5	24.5	40.0	40.1	**76.4**	**83.2**	**76.5**	**77.2**
Jul	17.6	14.0	23.3	22.9	30.6	25.4	40.5	39.9	**74.4**	**81.3**	**73.9**	**74.6**
Aug	17.0	14.0	23.0	23.1	28.4	24.4	38.1	38.3	**67.6**	**74.6**	**65.6**	**65.9**
Sep	14.7	13.9	21.8	22.3	23.5	23.1	34.0	34.8	**60.0**	**66.4**	**56.0**	**56.3**
Oct	12.6	14.2	17.8	19.1	19.0	22.4	26.6	28.4	**51.1**	**58.3**	**49.5**	**49.2**
Nov	7.7	14.1	12.1	13.7	11.5	21.2	17.7	19.9	**49.8**	**50.9**	**46.5**	**45.7**
Dec	6.5	13.8	8.5	8.6	9.6	20.4	12.5	12.9	**48.3**	**48.2**	**47.7**	**49.1**

Analysis done on monthly basis for Madison, Miami, Sacramento and Fresno

Table 6.2 ETC - FPC Comparison ($\beta = 60°$, $\phi = 45°$)

6.3 Fraction Diffuse Multiplier Calculation

In order to assess the effect IAMs have on the component of diffuse radiation, weighting factors are used for the IAMs. The weighting factors depend on the IAM itself, the cosine of the angle of incidence, and the surface area of a patch around the tail point of the input vector for each combination of γ and β. This patch around each point is obtained by specifying four additional points corresponding to four sets of γ and β angles, obtained by adding and subtracting a fixed number of degrees (2.5 in this case) to and from the γ and β angles for the original point under consideration. Each patch is a spherical quadrilateral which is divided into two spherical triangles as the areas of these spherical triangles are easily calculated (Tuma [1987]).

Thus, three matrices are required for the computation of a single *fraction diffuse multiplier* for a given geometry. These are a matrix of IAMs (similar to the one shown in

Table 6.3), a matrix of surface areas and a matrix of the cosines of the incidence angles corresponding to all the sets of γ and β used.

The fraction diffuse multiplier (F_D) is then calculated using,

$$F_D = \frac{\sum_i IAM(i)\,AREA(i)\cos\theta(i)}{\sum_i AREA(i)\cos\theta(i)} \qquad (6.1)$$

where i corresponds to a particular cell location in the three matrices.

6.4 Error Obtained in Using the Multiplicative Approach

Table 6.3 shows the matrix of the total hemispherical IAMs corresponding to 5° increments of γ and β obtained from the ray trace routine. Table 6.4 shows the error obtained in the calculation of the IAMs when the multiplicative method (Section 1.2) is used. The error shown is the difference (+ or -) between the total hemispherical IAMs and the IAMs calculated by the multiplicative algorithm.

Although the error incurred as a result of the multiplicative method is substantial only at the higher angles of incidence for the particular geometry analyzed, it is recommended that the total hemispherical IAMs be used whenever possible as they are accurate for any geometry.

Total Hemispherical Incidence Angle Modifiers
For Sun Family Collector with Diffuse Reflector (rho = 0.8) behind Absorber Tubes

γ \ β	0	5	10	15	20	25	30	35	40	45	50	55	60	65	70	75	80	85
0	1.00	0.99	0.99	0.99	0.98	0.97	0.96	0.96	0.96	0.95	0.95	0.93	0.89	0.86	0.80	0.72	0.58	0.63
5	0.99	0.98	0.98	0.99	0.98	0.98	0.98	0.98	0.97	0.96	0.95	0.93	0.90	0.85	0.80	0.69	0.60	0.60
10	1.01	1.00	1.00	0.99	1.00	0.99	0.99	0.98	0.98	0.99	0.96	0.95	0.91	0.87	0.81	0.71	0.62	0.62
15	1.03	1.01	1.01	1.01	1.01	1.01	1.00	1.01	0.99	0.99	0.98	0.96	0.93	0.88	0.83	0.75	0.62	0.61
20	1.04	1.04	1.04	1.03	1.03	1.03	1.02	1.02	1.01	1.01	0.99	0.98	0.96	0.92	0.86	0.75	0.66	0.61
25	1.07	1.07	1.06	1.06	1.05	1.06	1.05	1.05	1.05	1.03	1.02	1.01	0.97	0.94	0.91	0.78	0.67	0.60
30	1.10	1.10	1.10	1.09	1.08	1.09	1.08	1.08	1.08	1.07	1.06	1.04	1.01	0.97	0.93	0.85	0.70	0.65
35	1.14	1.14	1.14	1.13	1.14	1.12	1.12	1.12	1.10	1.10	1.09	1.08	1.06	1.01	0.96	0.87	0.75	0.65
40	1.19	1.19	1.19	1.20	1.18	1.18	1.18	1.17	1.17	1.15	1.14	1.13	1.12	1.08	1.01	0.94	0.79	0.69
45	1.24	1.25	1.23	1.22	1.23	1.22	1.23	1.22	1.23	1.21	1.19	1.19	1.17	1.13	1.08	1.01	0.85	0.71
50	1.27	1.27	1.27	1.26	1.26	1.25	1.25	1.26	1.26	1.25	1.24	1.22	1.21	1.19	1.13	1.06	0.92	0.76
55	1.32	1.31	1.32	1.30	1.31	1.32	1.30	1.32	1.29	1.29	1.29	1.28	1.26	1.23	1.20	1.12	0.97	0.80
60	1.38	1.38	1.38	1.37	1.37	1.36	1.38	1.35	1.37	1.36	1.35	1.32	1.33	1.30	1.26	1.21	1.08	0.85
65	1.45	1.45	1.45	1.45	1.46	1.45	1.44	1.44	1.44	1.43	1.44	1.43	1.40	1.40	1.36	1.33	1.19	0.93
70	1.59	1.57	1.57	1.59	1.56	1.58	1.57	1.57	1.57	1.57	1.58	1.56	1.55	1.53	1.50	1.48	1.33	1.12
75	1.79	1.78	1.77	1.80	1.79	1.79	1.76	1.75	1.76	1.78	1.75	1.76	1.75	1.75	1.73	1.70	1.58	1.37
80	2.09	2.10	2.10	2.08	2.09	2.09	2.08	2.09	2.08	2.09	2.06	2.08	2.08	2.05	2.09	2.09	2.05	1.87
85	2.79	2.81	2.76	2.84	2.76	2.81	2.79	2.77	2.76	2.83	2.79	2.69	2.82	2.74	2.95	2.84	2.92	3.01

γ = Angle of Incidence in the Transverse Direction
β = Angle of Incidence in the Longitudinal Direction

Table 6.3 Total Hemispherical Incidence Angle Modifiers Obtained as a Function of γ and β

Error obtained by using McIntyre's multiplicative method

γ \ β	0	5	10	15	20	25	30	35	40	45	50	55	60	65	70	75	80	85
0	0.00	0.00	0.00	0.00	0.00	0.00	0.00	0.00	0.00	0.00	0.00	0.00	0.00	0.00	0.00	0.00	0.00	0.00
5	0.00	0.00	0.00	0.01	0.01	0.01	0.03	0.03	0.01	0.02	0.01	0.01	0.01	0.00	0.01	-0.02	0.02	-0.03
10	0.00	0.00	0.00	-0.01	0.02	0.01	0.02	0.02	0.01	0.02	0.00	0.01	0.01	0.01	0.00	-0.01	0.03	-0.02
15	0.00	0.00	-0.01	-0.01	0.01	0.01	0.01	0.02	0.00	0.01	0.00	0.00	0.01	0.00	0.00	0.01	0.03	-0.04
20	0.00	0.02	0.01	0.00	0.02	0.02	0.02	0.02	0.01	0.02	0.01	0.01	0.03	0.03	0.03	0.00	0.05	-0.04
25	0.00	0.01	0.00	0.00	0.01	0.02	0.02	0.02	0.02	0.01	0.01	0.02	0.02	0.03	0.05	0.01	0.05	-0.07
30	0.00	0.01	0.01	0.00	0.01	0.02	0.01	0.02	0.02	0.02	0.02	0.02	0.03	0.03	0.05	0.06	0.06	-0.04
35	0.00	0.01	0.01	0.00	0.02	0.01	0.02	0.02	0.00	0.02	0.01	0.02	0.04	0.04	0.05	0.05	0.09	-0.07
40	0.00	0.02	0.01	0.02	0.02	0.02	0.03	0.03	0.02	0.02	0.02	0.03	0.05	0.06	0.06	0.08	0.10	-0.05
45	0.00	0.02	0.00	-0.01	0.02	0.02	0.03	0.04	0.03	0.03	0.02	0.04	0.06	0.07	0.09	0.12	0.13	-0.07
50	0.00	0.01	0.01	0.01	0.02	0.01	0.02	0.04	0.03	0.04	0.04	0.05	0.08	0.10	0.12	0.15	0.18	-0.04
55	0.00	0.01	0.01	-0.01	0.02	0.03	0.03	0.05	0.02	0.03	0.04	0.06	0.08	0.10	0.14	0.17	0.20	-0.03
60	0.00	0.02	0.01	0.00	0.02	0.01	0.05	0.03	0.04	0.04	0.04	0.04	0.10	0.12	0.16	0.22	0.28	-0.02
65	0.00	0.01	0.01	0.01	0.04	0.04	0.04	0.05	0.04	0.05	0.07	0.08	0.11	0.16	0.20	0.28	0.35	0.02
70	0.00	0.00	0.00	0.02	0.01	0.04	0.03	0.04	0.03	0.06	0.07	0.08	0.12	0.17	0.22	0.33	0.41	0.12
75	0.00	0.01	0.00	0.02	0.04	0.05	0.03	0.04	0.04	0.07	0.05	0.10	0.15	0.22	0.29	0.41	0.55	0.24
80	0.00	0.04	0.03	0.02	0.04	0.05	0.06	0.09	0.07	0.09	0.08	0.15	0.21	0.26	0.41	0.58	0.84	0.56
85	0.00	0.05	-0.01	0.08	0.03	0.10	0.09	0.09	0.07	0.17	0.15	0.11	0.32	0.35	0.72	0.83	1.30	1.25

γ = Angle of Incidence in the Transverse Direction
β = Angle of Incidence in the Longitudinal Direction

Table 6.4 Error Obtained by Using McIntyre's Multiplicative Method

6.5 Verification of Results

6.5.1 Experimental Verification

Experimental verification involves normal (Mason [1993]) and off-normal (Bickford [1994]) irradiated tests of the NEG Sun Family collector under the indoor solar simulator at Colorado State University.

For the normal incidence test an eight tube array (2 modules) was placed on a test stand with the collector aperture plane parallel to the plane of the irradiating lamps. The energy output, Q_{gain}, measured from the system under the test conditions is compared to the value obtained from a simulation run on TRNSYS. $(\tau\alpha)_n$ is adjusted in TRNSYS until the two values of Qgain are identical. The value of $(\tau\alpha)_n$ that results in the matching of the two Qgain values is taken to be the experimental $(\tau\alpha)_n$ for that particular collector configuration.

For the off-normal test, a four tube array positioned at two different combinations of γ and β under the simulator lamps was irradiated in a similar fashion. However, in addition to the $(\tau\alpha)_n$ which needs to be input, a matrix of IAMs corresponding to the NREL data set (Section 2.3) is also passed to the TRNSYS deck. Then the Q_{gain} value from the TRNSYS simulation is again made to match the value from the irradiance test by varying the value of $(\tau\alpha)_n$. The experimental value of $(\tau\alpha)_n$ for the collector is thereby determined.

The following are the results from the two tests compared to the $(\tau\alpha)_n$ value calculated using the ray trace routine:

Source of $(\tau\alpha)_n$	TRNSYS Calculation	Monte Carlo Calculation
$(\tau\alpha)_n$ (8 tube array)	0.652	0.656

Table 6.5 Comparison of $(\tau\alpha)_n$ for Normal Irradiance Test

The result from the TRNSYS calculation is 0.6% lower than the ray trace result.

Source of $(\tau\alpha)_n$	TRNSYS Calculation	Monte Carlo Calculation
$(\tau\alpha)_n$ (Test1,4 tube array, $\gamma = 28°, \beta = 8°$)	0.594	0.599
$(\tau\alpha)_n$ (Test2,4 tube array, $\gamma = 42.7°, \beta = 23.1°$)	0.559	0.599

Table 6.6 Comparison of $(\tau\alpha)_n$ for Off-Normal Irradiance Test

The result from the TRNSYS calculation for Test 1 is 0.8% lower than the ray trace result and is 6.7% lower for Test 2.

In both cases, the variations are well within the experimental tolerances and corroborate the validity of the ray trace calculations.

6.5.2 Flat Plate Collector Analysis

One additional way to verify the validity of the ray trace calculations is to calculate the IAMs for an FPC using the ray trace routine and then compare the results obtained with results obtained by using the analytical expression for angular dependence of the IAM for collectors with flat covers (Duffie and Beckman [1991]). This dependency is given by,

$$IAM = 1 + b_0\left(\frac{1}{\cos\theta} - 1\right) \tag{6.2}$$

where b_0 is a constant called the *incidence angle modifier coefficient*, and is generally a negative number. The relationship of Equation (6.2) does not apply at angles of incidence greater than 60°, however, it is good approximation for incidence angles less than 60°.

Figs. 6.21 and 6.22 show the comparison of the analyses at the same eight combinations of γ and β used earlier in section 6.1. The value of b_0 used in this analysis is -1.0 which corresponds to a flat plate collector with a single cover.

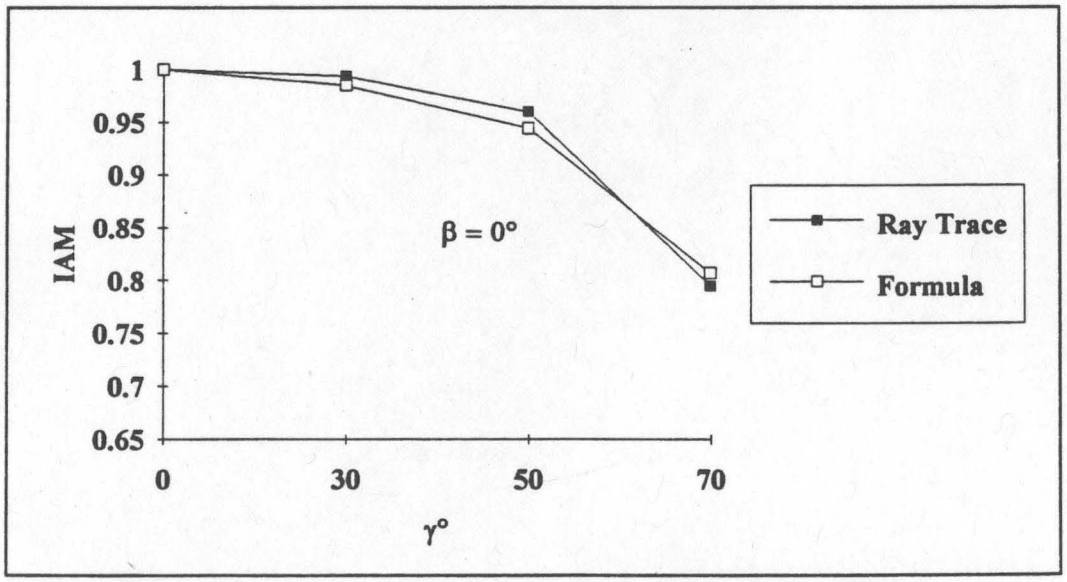

Figure 6.21 Comparison of Flat Plate IAMs ($\beta = 0°$)

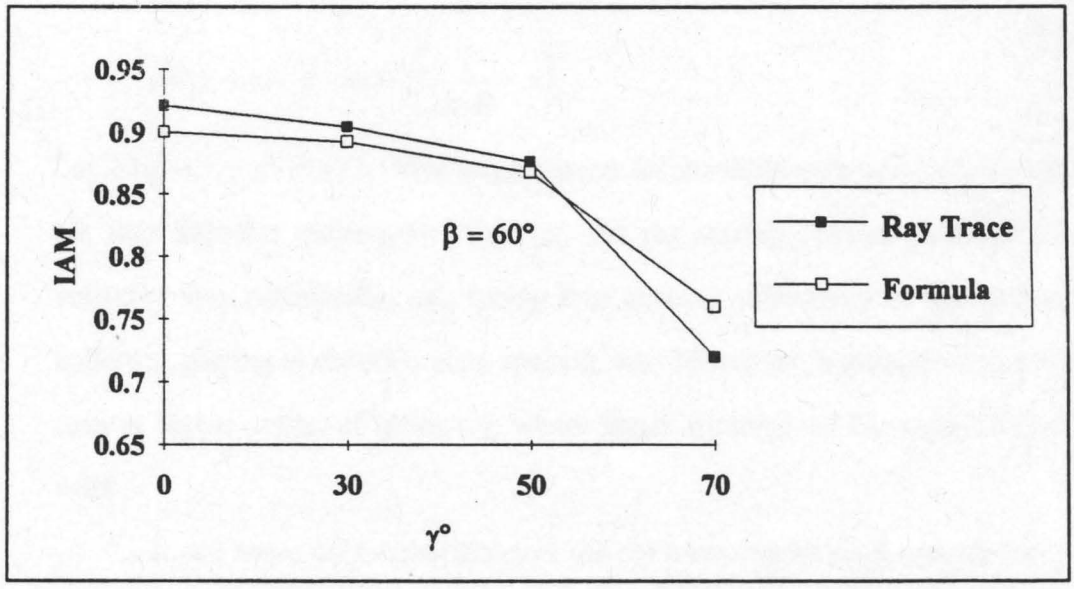

Figure 6.22 Comparison of Flat Plate IAMs (β = 60°)

The τα values from the ray trace run corresponding to the angles in Figs. 6.21 and 6.22 are given in Table 6.7.

γ (Degrees)	β (Degrees)	τα
0	0	0.829
30	0	0.823
50	0	0.795
70	0	0.658
0	60	0.763
30	60	0.749
50	60	0.726
70	60	0.596

Table 6.7 τα Values for FPC (Ray Trace Results)

A curve fit of the IAMs calculated by the ray trace results to Equation (6.2) yields the expression,

$$IAM = 1.019 - 0.117\left(\frac{1}{\cos\theta} - 1\right) \tag{6.3}$$

i.e., a b_0 value of -0.117. This is one reason for the difference in the IAMs obtained from the two different techniques. Further, the ray tracing routine involves modeling the collector very realistically, i.e., taking into account reflectivity of the side walls of the collector, glazing to absorber plate spacing, etc. Moreover, a greater variation in results is seen at higher angles of incidence, where the relationship of Equation (6.2) is no longer valid.

It can hence be summarized that the ray trace results yield accurate results that are applicable to any collector geometry.

CHAPTER SEVEN

CONCLUDING REMARKS

7.1 Summary

The Monte Carlo ray tracing technique provides an inexpensive and elegant method of determining the optical efficiencies of complex solar collector geometries with a reasonably high degree of accuracy. The results from the ray tracing routine have been verified against both experimental results, in the case of the NEG Sun Family collector, and against a theoretical model, in the case of a flat plate collector. The CSG module of the code allows the user to define the collector geometry in a simple and accurate manner and a single collector data file is required for visualization of the geometry as well as for use as input to the ray tracing routine. The multiplicative approach works well for (γ,β) combinations of less 40°, where the error incurred is no greater than 4%. However, at combinations greater than 40°, the error gradually increases, and reach values of 12-15%, and gets as high as 41% for a combination of (85°,85°). The energy coming from radiation at these higher angles of incidence is not as great as it is at lower angles of incidence, but the contribution is not negligible. Moreover, a substantial amount of effort is required to generate the biaxial IAMs. The additional effort needed to generate the entire IAM field using the method described in this thesis is not very much greater. It is therefore recommended that the total hemispherical IAMs be generated whenever possible using the ray tracing program as they are accurate for any collector configuration and the uncertainty of the applicability of the multiplicative approach is thereby eliminated.

Currently, off-incidence tests are difficult to conduct on the indoor solar simulator at CSU as the uniformity of the irradiance distribution may not satisfy the American

Society of Heating, Refrigerating and Air Conditioning Engineer's (ASHRAE) standard for uniformity and collimation of simulated irradiance when large collector areas are encountered and if the collector slope angles are large. In such cases, the ray trace routine can be used to give accurate estimates of the value of $(\tau\alpha)_n$, etc.

The optical performance of the NEG Sun Family collector module is definitely enhanced with the use of a reflective back plane. The four-sided box analysis, for a collector slope angle of 60°, shows that there is considerable radiation available for collection from the back and the sides of the collector. However, this increase in radiation availability is only significant at higher slope angles. For collector slopes greater than 50°, it would probably serve just as well to use the collector module without a reflective back plane. This would allow more radiation to reach the collector from the back side. However, in most cases where the collector slopes are less than 50°, it is recommended that a reflective back plane be used.

7.2 Recommendations for Further Work

The code is currently being modified to provide a weighted diffuse reflection model, i.e., where the probability of reflection is proportional to $\cos^r\theta$. The present diffuse reflection model is probably sufficiently accurate, but a comparison of results from the two different models would be of some interest.

Although the user can now define the collector geometry and visualize it without undue effort, the interface is not very "user friendly." Rotation angles, object dimensions, etc. cannot be modified dynamically, and a separate data file is needed for each visualization run. The current hardware capabilities do not facilitate an improvement in this process, and it would thus be better if the code could be modified to run on faster machines with superior graphics capabilities such as the Silicon Graphics workstations.

New geometries and modifications to existing geometries should be analysed to determine their optical efficiencies and evaluate the effectiveness of any new design

features. A new NEG Sun Family module has been developed which is equipped with a reflector. This is one of the geometries which will be studied as part of on going work in this area of study.

BIBLIOGRAPHY

Bickford, C., (1994). *Personal Communication.*

Chow, S. P., G. L. Harding, B. Window, and K. J. Cathro, *Solar Energy*, **32**, p. 251 (1984). "Effects of Collector Components on the Collection Efficiency of Tubular Evacuated Collectors with Diffuse Reflectors."

Dempsey, S., (1992). Distributed System Implementation. *Personal Communication.*

Duffie, J. A., and W. A. Beckman, (1980). *Solar Engineering of Thermal Processes, 2nd Edition.* John Wiley & Sons, New York.

Felske, J. D., Technical Note, *Solar Energy*, **22**, pp. 567-570 (1979). "Analysis of an Evacuated Cylindrical Solar Collector."

Glassner, A. J., (1989). *An Introduction to Ray Tracing.* Academic Press, San Diego.

Klein, S. A. et al., (1992). "TRNSYS- A Transient System Engineering Program," Engineering Experiment Station Report 38-13, Solar Energy Laboratory, University of Wisconsin-Madison.

Knappmiller, K., (1990). "Computation of Total Hemispheric Incident Angle Modifiers for Solar Collectors," Master's Thesis, Colorado State University.

Maltby, J. D. and P. J. Burns, *Numerical Heat Transfer*, (1989). "Performance, Accuracy and Convergence in a Three-Dimensional Monte Carlo Radiative Heat Transfer Simulation."

Maltby, J. D., (1990). "Analysis of Electron Heat Transfer Via Monte Carlo Simulation," Ph.D. Dissertation, Colorado State University.

Mason, A. A., (1993). "Stratification and Performance Prediction in an Evacuated Tube, Integral Storage Collector," Master's Thesis, Colorado State University.

McIntire, W. R., *Solar Energy*, **29**, No. 4, pp. 315-322 (1982). "Factored Approximations for Biaxial Incident Angle Modifiers."

Modest, M., (1993). *Radiative Heat Transfer.* McGraw Hill, New York.

Press, W. H., S. A. Teukolsky, W. T. Vellerling, and B. P. Flannery, (1992). *Numerical Recipes in C, 2nd Edition*. Cambridge University Press.

Roth, S. D., *Comput. Graph. Image Process*, **18** (2), pp. 109-144 (1982). "Ray Casting for Modeling Solids."

Theunissen, P-H., and W. A. Beckman, *Solar Energy*, **35**, No. 4, pp. 311-320 (1985). "Solar Transmittance Characteristics of Evacuated Tubular Collectors with Diffuse Back Reflectors."

Tuma, J. J., (1987). *Engineering Mathematics Handbook, 3rd Edition*. McGraw Hill, New York.

Window, B and J. Zybert, *Solar Energy*, **26**, pp. 325-331 (1981). "Optical Collection Efficiencies of Arrays of Tubular Collectors with Diffuse Reflectors."

APPENDIX A

A.1 Software Used

The programs needed to use the ray trace routine are on the 3.5" IBM compatible diskette included at the back of this thesis manuscript. The software required is divided into three sections; the Display routine, the IAM routine and the Network Distribution routine.

A.1.1 Display Routine

The display routine has been developed on the Borland C/C++ 2.0 programming environment (using 'Project' files) on an IBM compatible PC. The executable file required to run the display routine is:

csg.exe

This executable should run on any IBM compatible PC which has 'vga' or 'super vga' color. The files **egavga.bgi** and **limits.dat** (also provided) must be present in the working directory. All the program files required to create the executable are also provided should the user wish to understand the programs better or add other capabilities to the code, etc.

There are some standard Borland library files required to compile the programs. These are files declared at the start of each program using:

#include <filename>

In addition to these there are other header files declared using:

#include "filename"

Care should be taken to ensure that all files needed are located in the same directory or that the appropriate path to the necessary files is provided. The C files and header files required to create the executable are as follows:

C-Files: **csgmain.c** **csgbody.c** **csggraph.c** **allocmat.c** **vectops.c**

Header Files: **allocmat.h** **vectops.h** **types.h**

All of the files listed above are compressed into a single file:

display.zip

This file can be exploded into its different components using the **unzip** command on any IBM compatible PC. The **zip.exe** and **unzip.exe** files are also provided. Chapter 4 (Modeling Scheme) describes the user coordinate system and other issues critical to the display routine.

A.1.2 IAM Routine

The programs for the calculation of the $\tau\alpha$ product were developed on the same Borland C/C++ 2.0 environment as the display routine. However, in order to exploit the networking capabilities of the UNIX operating system, the programs were then recompiled for the DEC 3100/5000 workstations on the LANCE network. All the C files have been written using ANSI standard C as so they may be recompiled using practically any compiler on any platform (UNIX or DOS). All the files needed for the implementation of the IAM routine are compressed into the single file:

iam.zip

This file may be 'unzipped' either on an IBM compatible PC or on an UNIX workstation. The C files and header files required to create the executable are as follows:

C-Files: **iammain.c** **csgbody.c** **random.c** **allocmat.c** **vectops.c**

Header Files: **allocmat.h** **vectops.h** **types.h** **random.h**

All the C files are compiled together using a 'makefile.' The makefile is also provided. Upon compilation, the resultant executable is called:

program

The **program** executable provided has been compiled on the DEC 3100/5000 workstations at LANCE, and therefore will only work these machines. Recompilation will be necessary if the programs are used on any other platform.

Running **program** requires either 'command line' or 'stdin' input of the following five variables:

X coordinate of input vector

Y coordinate of input vector

Z coordinate of input vector

Convergence Accuracy

Random number generator seed

For example, the stdin input (at the system prompt (%)) for normal incidence, at 1% accuracy with an initial seed taken as 252 is:

% program 0.0 0.0 1.0 0.01 252 > output.001

Here the output from the program is being redirected into a file called output.001. A separate line such as above, is required for each new input direction (with the appropriate input coordinates), and a new seed. In addition to this input, there should also be a file in the working directory called:

col.dat

This is the collector data file as described in Section 4.2 (Chapter 4).

Running **program** yields an output line, which consists of the five variables discussed above, and the two fractions which the program calculates for each direction of input radiation. Only the fraction in the last column of the output line is of interest and is the $\tau\alpha$ product for that particular angle of incident radiation. The IAMs are then calculated by dividing each of the $\tau\alpha$ values obtained for each angle of incoming radiation by the value of $\tau\alpha$ for normal incidence, i.e., $(\tau\alpha)_n$. To do this, all the **output.***** should be concatenated to give a single file called **iaminput**, which is then passed through the IAM calculation routine. This is done with the help of the program

iamrun.f

which has been compiled on the DEC 3100/5000 workstations to give the executable

iamrun

The user is required to input the number of lines in the **iaminput** input file, and the output from this run is placed in a file called **iam.out**. This file contains the IAMs for the different angles of incident radiation for the particular collector being analyzed.

A.1.3 Network Distribution Software

The executable files needed to use the distribution software on LANCE are included in the file

dist.zip

Again, 'unzipping' this file will yield the separate files needed. It should be noted by the reader that the software used for the distribution of the different vectors on multiple machines was developed by Steve Dempsey [1992] in unofficial capacity, and is therefore not supported by the LANCE administrators. Included in the **dist.zip** file is a set of instructions for running the network distribution routine, etc.

In the event that the distribution software does not perform as expected, the user can revert to using UNIX 'script' files similar to those described by Knappmiller [1990].